Limitation of phosphate assimilation maintains cytoplasmic magnesium homeostasis

Roberto E. Bruna[1,2], Christopher G. Kendra[1,2], Eduardo A. Groisman[3,4], Mauricio H. Pontes[1,2]*

[1] *Department of Pathology and Laboratory Medicine, and* [2] *Department of Microbiology and Immunology, Penn State College of Medicine, 500 University Drive, P.O. Box 17033, Hershey, PA, 17033, USA*

[3] *Department of Microbial Pathogenesis, Yale School of Medicine, 295 Congress Avenue, New Haven, CT 06536, USA*

[4] *Yale Microbial Sciences Institute, P.O. Box 27389, West Haven, CT, 06516, USA*

*Address correspondence to Mauricio H. Pontes, mpontes@pennstatehealth.psu.edu

Classification

Biology, Microbiology

Keywords

Phosphate, ATP, Magnesium, MgtC, *Salmonella*

Author Contributions

R.E.B., C.G.K., E.A.G. and M.H.P. designed research; R.E.B., C.G.K. and M.H.P. performed research; R.E.B., C.G.K. and M.H.P. analyzed data; E.A.G. and M.H.P. contributed reagents/analytic tools; R.E.B. and M.H.P. wrote the paper.

Abstract

Phosphorus (P) is an essential component of several core biological molecules. In bacteria, P is mainly acquired as inorganic orthophosphate (Pi). Once in the cytoplasm, Pi is incorporated into adenosine triphosphate (ATP), which exists primarily as a Mg^{2+} salt. Notably, whereas P is essential, excess of cytosolic Pi hinders growth. Here we demonstrate that cytotoxic effects of excessive Pi uptake result from its assimilation into ATP and subsequent disruption of Mg^{2+} dependent processes. We show that *Salmonella enterica* cells experiencing cytoplasmic Mg^{2+} starvation restrict Pi uptake, thereby limiting the availability of an ATP precursor. This response prevents excessive ATP synthesis, overproduction of ribosomal RNA, chelation of free cytoplasmic Mg^{2+} and the destabilization of Mg^{2+}-dependent core processes that ultimately hinder bacterial growth and leads to loss of cellular viability. We demonstrate that, even when cytoplasmic Mg^{2+} is not limiting, excessive Pi uptake leads to increased ATP synthesis, depletion of free cytoplasmic Mg^{2+}, inhibition of translation and growth. Our results establish that bacteria must restrict Pi uptake to prevent the depletion of cytoplasmic Mg^{2+}. Furthermore, they provide a framework to understand the molecular basis of Pi cytotoxicity and reveal a regulatory logic employed by bacterial cells to control P assimilation.

Importance

Phosphorus (P) is essential for life. As the fifth most abundant element in living cells, P is required for the synthesis of an array of biological molecules including (d)NTPs, nucleic acids and membranes. Organisms typically acquire environmental P as inorganic phosphate. While essential for growth and viability, excessive intracellular Pi is toxic for both bacteria and eukaryotes.

Using the bacterium *Salmonella enterica* as a model, we demonstrate that Pi cytotoxicity is manifested following its assimilation into ATP, which acts as a chelating agent for intracellular cations, most notably, Mg^{2+}. These results identify physiological processes disrupted by excessive Pi and elucidate a regulatory logic employed by bacteria to prevent uncontrollable P assimilation.

Introduction

Phosphorus (P) is an intrinsic component of a large number of biological molecules, including membrane lipids, nucleotides and nucleic acids. This element is required for many central biological functions, including (1) the formation of cellular boundaries, (2) the storage and transfer of chemical energy, (3) the integration and propagation of information in signal transduction pathways, and (4) the storage, transmission and expression of genetic information. Bacterial cells mainly uptake P as inorganic phosphate (PO_4^{-3}; Pi), which is then assimilated in the cytoplasm via its incorporation into adenosine triphosphate (ATP). ATP functions as the main cellular P-carrier molecule, mediating both the transfer of Pi among biological molecules and the release of chemical energy to power energy-dependent processes (1). Interestingly, while the assimilation of P is essential, excessive cytoplasmic Pi is toxic (2–7). This implies that cells must tightly regulate Pi acquisition and utilization to avoid self-poisoning. Here, we elucidate how bacterial cells coordinate Pi acquisition and consumption to prevent deleterious effects of unbalanced Pi metabolism.

Following assimilation, negative charges from Pi groups in biomolecules are neutralized by positively charged ionic species present in the cytoplasm. As such, the majority of cytoplasmic ATP exists as a salt with positively charged

82 magnesium (Mg^{2+}), the most abundant divalent cation in living cells. Indeed,
83 this ATP:Mg^{2+} salt, rather than the ATP anion, functions as the substrate for
84 most ATP-dependent enzymatic reactions (8–10). In enteric bacteria, ATP
85 stimulates the transcription of ribosomal RNAs (rRNA) (11, 12). The synthesis
86 and activity of ribosomes consume the majority of the ATP in the cell (13).
87 During ribosome biogenesis, negative charges from Pi groups in the rRNA
88 backbone chelate large amounts of Mg^{2+} ions. This process reduces electrostatic
89 repulsion among Pi groups in the rRNA backbone, enabling the folding and
90 assembly of functional ribosomes. Not accidentally, ATP and rRNA constitute
91 the largest cytoplasmic reservoirs of Pi *and* Mg^{2+} (9, 11, 13–18). Given this
92 inherent connection between Pi and Mg^{2+}, we wondered if cytotoxic effects of
93 excessive Pi uptake result from its assimilation into ATP and subsequent
94 disruption of Mg^{2+} dependent processes in the cytoplasm.
95 In the Gram negative bacterial pathogen *Salmonella enterica*, prolonged
96 growth in media containing limiting Mg^{2+} induces cytoplasmic Mg^{2+} starvation.
97 This stress promotes the expression of the MgtA, MgtB and MgtC membrane
98 proteins (19–22). MgtA and MgtB function as high-affinity, ATP-dependent
99 Mg^{2+} importers, increasing the Mg^{2+} concentration in the cytoplasm (23, 24). By
100 contrast, MgtC decreases intracellular ATP levels (25), thereby reducing rRNA
101 synthesis, lowering steady-state levels of ribosomes, and slowing translation
102 rates (26). This response reduces levels of assimilated P and, consequently, the
103 quantity of Mg^{2+} required as a counter-ion, effectively preventing the depletion
104 of cytoplasmic Mg^{2+} that is required for the stabilization of existing ribosomes
105 and the maintenance of other vital Mg^{2+}-dependent cellular processes (19, 26,
106 27). Interestingly, MgtC is also expressed during replication of *Salmonella* inside
107 mammalian macrophages, where it promotes bacterial survival and enables the
108 establishment of systemic infections (28, 29). In macrophages, MgtC inhibits the

activity of *Salmonella*'s F_1F_o ATP synthase, thereby hindering ATP production via oxidative phosphorylation (30, 31). Yet, mutations in single amino acid residues of the MgtC protein abolish intramacrophage survival of *Salmonella* without affecting its growth and viability during cytoplasmic Mg^{2+} starvation. This indicates that MgtC operates by distinct mechanisms in these two growth conditions (32).

In this paper, we reveal that the limitation of phosphate uptake is essential to maintain cytoplasmic Mg^{2+} homeostasis. We establish that during cytoplasmic Mg^{2+} starvation, MgtC lowers ATP levels by inhibiting Pi uptake, thus limiting an ATP precursor instead of interfering with its enzymatic generation. We demonstrate that, counterintuitively, limitation of exogenous Pi availability rescues translation, promotes growth and restores viability to an *mgtC* mutant. We provide genetic and functional evidence that MgtC hinders the activity of an uncharacterized transporter, which functions as the main Pi uptake system in *Salmonella* and likely other bacterial species. Finally, we establish that even at physiological levels of cytoplasmic Mg^{2+}, Pi exerts its toxicity following its incorporation into ATP and subsequent disruption of Mg^{2+}-dependent processes. While providing a conceptual framework to understand the underlying basis of Pi cytotoxicity, a phenomenon observed in both bacteria and eukaryotes (3–7, 33–36), our results uncover a regulatory logic employed by bacterial cells for the global control of P assimilation.

Results

An F_1F_o synthase-independent mechanism limits ATP accumulation during low cytoplasmic Mg^{2+} stress

In living cells, ATP exists as a Mg^{2+} salt (10, 13). When cells are faced with limiting cytoplasmic Mg^{2+} concentrations, they reduce ATP levels to free Mg^{2+} ions that are required for other cellular processes, such as the assembly of ribosomes (26, 27). In *Salmonella*, this reduction in ATP levels is accomplished by the MgtC membrane protein, which is expressed in response to a number of physiological signals generated by cytoplasmic Mg^{2+} starvation (19, 21, 25, 37, 38). MgtC is also expressed during *Salmonella* replication in mammalian macrophages, where it promotes bacterial survival (28, 29). In macrophages, MgtC functions by inhibiting the activity of *Salmonella*'s F_1F_O ATP synthase, the enzyme responsible for ATP synthesis via oxidative phosphorylation (30). Notably, a *Salmonella mgtC atpB* double mutant strain—containing a genetically inactive ATP synthase—was also reported to harbor lower ATP levels than an *mgtC* single mutant strain during cytoplasmic Mg^{2+} starvation (30). This result led to the notion that MgtC also prevents a non-physiological rise in ATP levels by inhibiting the F_1F_O ATP synthase when *Salmonella* experiences cytoplasmic Mg^{2+} starvation (30, 39, 40). However, because the biochemical function of MgtC during cytoplasmic Mg^{2+} starvation can be genetically separated from its function during intramacrophage replication (32), we sought to reexamine the interpretation of the aforementioned experimental results.

The F_1F_O ATP synthase uses the proton motive force, generated by the respiratory electron transport chain, to synthesize ATP from ADP and Pi (41, 42). Consequently, an *mgtC atpB* double mutant (or any other strain lacking a functional ATP synthase) relies exclusively on fermentative pathways to produce ATP via substrate-level phosphorylation (43). Interestingly, the aforementioned lower ATP levels observed in a *Salmonella mgtC atpB* double mutant were obtained during growth on medium containing glycerol as the carbon source (30). Given that the fermentation of glycerol is extremely

inefficient (44, 45), we reasoned that lower ATP levels in the *mgtC atpB* double mutant could simply reflect an inability of this strain to efficiently ferment glycerol. To test this notion, we compared ATP levels in wild-type, *mgtC*, *atpB* and *mgtC atpB Salmonella* strains grown in minimal medium containing readily fermentable glucose as the carbon source and low (10 μM) Mg^{2+}, to induce cytoplasmic Mg^{2+} starvation (20, 21). Consistent with our hypothesis, we established that after 5 h of growth, when cytoplasmic Mg^{2+} becomes limiting (26), *mgtC* and *mgtC atpB* strains had 42 and 29-fold higher ATP levels relative to their $mgtC^+$ isogenic counterparts, respectively (Fig. 1*A*). Hence, a second mutation in *atpB* does not abrogate the intracellular ATP accumulation in an $mgtC^-$ background provided cells are fed with glucose as the carbon source.

To further test our hypothesis, we compared ATP levels in wild-type, *mgtC*, *atpB* and *mgtC atpB* strains at 90 min following a nutritional downshift from medium containing high (10 mM) Mg^{2+} and glucose, to media lacking Mg^{2+} and containing one of various carbon sources (Fig. 1*B*). In agreement with our hypothesis, there was a predictable trend in ATP levels among these strains. That is, we determined that during cytoplasmic Mg^{2+} starvation the *mgtC* strain had high ATP levels regardless of the carbon source (Fig. 1*C*). By contrast, the *mgtC atpB* strain had increased ATP levels during growth on readily fermentable carbon sources (glucose, gluconate, arabinose or pyruvate), but was unable to do so during growth on inefficiently fermentable glycerol (Fig. 1*B-C*). As a control, all the strains tested displayed similar ATP levels when resuspended in high Mg^{2+}, glucose-containing medium (Fig. 1*C*). Taken together, these results indicate that the low ATP levels previously observed in an *mgtC atpB* strain experiencing cytoplasmic Mg^{2+} starvation (30) are caused by an inability to efficiently ferment glycerol, as opposed to an inability to inhibit the F_1F_O ATP synthase. Furthermore, these results indicate that MgtC inhibits

multiple ATP-generating reactions in the cell, not only that one which is carried out by the F_1F_O complex.

MgtC inhibits inorganic phosphate acquisition and *ipso facto* limits ATP synthesis during cytoplasmic Mg^{2+} starvation

ATP can be synthesized by several catabolic reactions in the cell (46–48). How then can MgtC control the activity of multiple ATP-producing enzymatic reactions? We reasoned that regardless of the identity of the enzymes catalyzing ATP formation, the overall rate of ATP synthesis in the cell could be restricted by the availability of substrates. MgtC could, therefore, function by inhibiting the synthesis or acquisition of an ATP precursor. Interestingly, at the onset of cytoplasmic Mg^{2+} starvation, a temporary shortage in the levels of free cytoplasmic Mg^{2+} destabilizes the bacterial ribosomal subunits (26). The resulting decrease in translation efficiency reduces ATP consumption and, consequently, the recycling of Pi from ATP. This lowers the concentration of cytoplasmic Pi, transiently activating the cytoplasmic Pi-starvation sensing PhoB/PhoR two-component system in *Salmonella* (15). Three lines of evidence led us to hypothesize that MgtC prevents ATP synthesis by limiting Pi influx into the cell. First, PhoB/PhoR activation is hampered in an *mgtC* mutant, indicating that this strain experiences excess cytoplasmic Pi (15). Second, *mgtC* and *mgtC atpB* strains have higher intracellular steady-state Pi levels than wild-type and *atpB Salmonella* strains (Fig. 2*A*), confirming that MgtC prevents the accumulation of intracellular Pi in an *atpB*-independent fashion. Third, when Mg^{2+} and Pi are abundant, ectopic expression of MgtC from a plasmid induces PhoB/PhoR activation, further suggesting that MgtC causes a shortage in cytoplasmic Pi (Fig. S1) (15).

To test the aforementioned hypothesis, we measured transport of radiolabeled Pi (^{32}Pi) following MgtC expression from its native chromosomal location in response to cytoplasmic Mg^{2+} starvation. We established that *mgtC* cells accumulated four times more radioactivity than the isogenic wild-type strain after 30 min of growth in the presence of ^{32}Pi (Fig. 2*B*). This indicated that the increased steady-state intracellular Pi levels observed for *mgtC* and *mgtC atpB* mutants (Fig. 2*A*) arises from the uptake of extracellular Pi, as opposed to increased Pi release from intracellular sources. [Note that all ^{32}Pi transport assays were performed in the presence of cold Pi, at a molar ratio of 1:25 (^{32}Pi:Pi), to prevent the expression of the PstSCAB Pi transporter resulting from lack of Pi in the growth medium (1). The influx of Pi observed in the assays is underestimated (see Discussion and Materials and Methods)].

If MgtC functions to restrict cytoplasmic Pi availability, and Pi is required for ATP synthesis, we posited that the increased ATP levels in an *mgtC* mutant, but not in wild-type *Salmonella*, could be regulated by the availability of Pi in the growth medium. To test this prediction, we measured ATP levels in wild-type and *mgtC* cells grown in minimal media with low Mg^{2+} and decreasing concentrations of exogenous Pi. [Note that bacteria are able to grow in medium lacking exogenous Pi, due to the residual Pi content present in the mixture of casamino acids supplemented to the culture medium (see Materials and Methods)]. Strikingly, we established that, during cytoplasmic Mg^{2+} starvation, the ATP levels in an *mgtC* mutant could be reduced by decreasing exogenous Pi from 500 to 0 μM (Fig. 2*C*). By contrast, ATP levels in wild-type cells remained invariably low (Fig. 2*C*). Importantly, in the absence of exogenous Pi, wild-type and *mgtC* cells had similar levels of ATP (Fig. 2*C*). Taken together, these results indicate that MgtC controls ATP synthesis by limiting cellular Pi uptake.

240

241 **MgtC inhibits a non-canonical Pi transport system**

242 *Salmonella enterica* encodes two *bona fide* Pi import systems: *pitA* and *pstSCAB*
243 (Fig. 3*A*). While PitA functions as a metal:phosphate (M:Pi)/proton symporter
244 (1, 49–51), PstSCAB works as a high affinity, ATP-dependent Pi transporter
245 (Fig. 3*A*) (1, 6, 51, 52). In addition to *pitA* and *pstSCAB*, *Salmonella* also harbors
246 an *yjbB* homolog, which encodes a sodium/phosphate symporter. Whereas
247 YjbB has been shown to promote Pi export (53), we performed experiments
248 under a cautious assumption that this protein may also be able to import Pi
249 (Fig. 3*A*).

250 To directly test the role of MgtC on the inhibition of PitA, PstSCAB or YjbB,
251 we measured ^{32}Pi uptake following ectopic MgtC expression in the wild-type
252 and a *pitA pstSCAB yjbB* triple mutant (3ΔPi) strains. In wild-type cells,
253 harboring all known Pi transport systems, MgtC expression led to a mild (17%)
254 decrease in ^{32}Pi uptake when compared with the empty vector control (Fig. 3*B*).
255 By contrast, ectopic expression of MgtC reduced Pi uptake by 70% in the 3ΔPi
256 background, relative to the vector control (Fig. 3*B*), indicating that MgtC
257 decreases Pi influx in a *pitA pstSCAB yjbB*- independent manner. In support of
258 these results, a 3ΔPi is able to grow using Pi as the sole P source (Fig. 3*C*),
259 indicating that a yet unidentified transporter imports Pi into the cytoplasm to
260 support the growth of this *Salmonella* strain.

261 Two additional lines of evidence indicated that MgtC inhibits the activity of
262 a non-canonical Pi transporter. First, because MgtC expression causes a
263 shortage in cytoplasmic Pi (Fig. 2 and 3*B*), ectopic expression of MgtC elicits a
264 dose-dependent activation of the PhoB/PhoR two-component system and
265 transcription of the PhoB-activated PstSCAB transporter (Fig. S1) (15). Hence,

deletion of the MgtC-targeted Pi transporter should result in a constitutively high *pstS-gfp* activity that is irresponsive to MgtC expression. In other words, deletion of the Pi transporter should be epistatic to the effect of MgtC expression on PhoB/PhoR activation levels. Consistent with the notion that MgtC inhibits a non-canonical Pi transporter, we determined that expression of MgtC (either ectopically in medium containing 250 μM Mg^{2+} or natively in medium containing 10 μM Mg^{2+}) induced *pstS* transcription in *pitA* and *yjbB* single and double mutant strains (Fig. 3*D-E*). [We purposely did not carry out this epistatic analysis with the *pstSCAB* mutant for two reasons. First, the PstSCAB transporter participates in the regulation of the PhoB/PhoR two-component system through a physical interaction (54). Consequently, inactivation of the transporter through mutations in *pst* genes leads to PhoB/PhoR hyperactivation, effectively preventing signal transduction (1, 3, 54, 55). Second, we reasoned that it would be unlikely for cells to have evolved a regulatory circuit whereby MgtC inhibition of PstSCAB transporter activity would promote PstSCAB expression (Fig. S1) (15), requiring more MgtC protein, *ad infinitum*]. Second, we posited that deleting the MgtC-inhibited transporter in an *mgtC* background should abolish its exacerbated ATP accumulation (Fig. 2*C*). However, mutations in either *pitA*, *pstSCAB* or *yjbB* did not lower the intracellular ATP levels of an *mgtC* mutant (Fig. 3*F*). In sum, these experiments indicate that MgtC inhibits Pi uptake by targeting an unidentified Pi transporter.

Phosphate limitation rescues the translation and growth defects of an *mgtC* mutant experiencing cytoplasmic Mg^{2+} starvation

The increased ATP levels in an *mgtC* mutant experiencing cytoplasmic Mg^{2+} starvation causes ribosomal assembly defects, presumably because Mg^{2+} ions

293 required for ribosome stabilization are bound to ATP molecules (26). This
294 results in inefficient translation, growth arrest and a loss of viability (19, 26), all
295 of which can be reversed by enzymatic hydrolysis of ATP (26, 27). Given that
296 MgtC lowers ATP synthesis by inhibiting Pi acquisition (Fig. 2*A*, 2*C* and 3*B*), we
297 reasoned that the translation, the growth defects and the loss of viability of an
298 *mgtC* mutant would also be rescued by limiting the access of cells to Pi. To test
299 this notion, we measured translation rates in the wild-type and *mgtC* strains
300 experiencing cytoplasmic Mg^{2+} starvation in the presence of 500 or 0 μM
301 exogenous Pi. As predicted, wild-type and *mgtC* strains showed similar
302 translation rates in the absence of exogenous Pi (Fig. 4*A*-*B*). By contrast, during
303 growth at 500 μM Pi, the translational rate of the *mgtC* mutant was 4.7-fold
304 reduced in comparison with wild-type levels (Fig. 4*A*-*B*).
305 Next, we measured the effect of reducing exogenous Pi on growth and
306 viability of strains grown in low Mg^{2+} medium. We established that steadily
307 decreasing exogenous Pi in the growth medium from 500 to 0 µM progressively
308 increased the growth of the *mgtC* mutant strain (Fig. 4*C*). Remarkably, in the
309 absence of exogenous Pi, the *mgtC* mutant displayed growth yield and kinetics
310 indistinguishable from that of the wild-type strain (Fig. 4*C*). Furthermore,
311 during growth in medium lacking Pi, the loss of viability observed in the *mgtC*
312 mutant (19) was suppressed, and the mutant maintained the same number of
313 colony forming units (CFU) per optical density unit (OD_{600}) as the wild-type
314 strain (Fig. 4*D*). As expected, the growth of wild-type and *mgtC* mutant
315 cultures in medium containing 500 µM Pi were indistinguishable when Mg^{2+}
316 was made abundant by raising its concentration from 10 to 500 µM (Fig. 4*C*).
317 Altogether, these results establish that MgtC functions to prevent cytotoxic
318 effects resulting from excessive Pi uptake.

Pi cytotoxicity results from its exacerbated assimilation into ATP and subsequent chelation of Mg^{2+} during growth under conditions of high Mg^{2+}

Excessive Pi uptake has been known to hinder bacterial growth in conditions where access to extracellular Mg^{2+} is not limiting and, consequently, cells are not anticipated to experience cytoplasmic Mg^{2+} starvation (3, 7). For instance, in *E. coli*, mutations that increase PstSCAB activity or expression cause heightened Pi uptake and growth inhibition (1–4). Given the aforementioned experimental results, we hypothesized that excess Pi would exert its cytotoxicity following its incorporation into ATP, and subsequent chelation of essential cations, particularly Mg^{2+}.

According to this hypothesis, PstSCAB overexpression should promote phenotypes caused by cytoplasmic Mg^{2+} starvation—i.e. elevated ATP levels, inhibition of translation and growth, and induction of MgtC expression (19, 25, 26). Additionally, these phenotypes should be rescued by increasing the availability of free cytoplasmic Mg^{2+}, through the provision of excess Mg^{2+} in the growth medium, or the reversal of P assimilation through enzymatic hydrolysis of ATP (19, 26, 27). To test this notion, we initially measured ATP levels and growth of wild-type cells following ectopic over-expression of the PstSCAB transporter from a plasmid. During growth in medium containing high (10 mM) Pi and intermediate (0.1 mM) Mg^{2+} levels, cells do not typically experience cytoplasmic Mg^{2+}starvation (20, 21) and, consequently, do not express MgtC (Fig. 6*A*). Under these growth conditions, PstSCAB overexpression caused approximately a 4-fold increase in ATP levels in comparison to control strains harboring either an empty vector or a plasmid expressing the inner membrane protein PmrB (Fig. 5*A*). Notably, this rise in

ATP levels was accompanied by reductions in growth rate and growth yield, two phenotypes not observed in the control strains (Fig. 5*B*).

Two lines of evidence indicated that the growth defect resulting from PstSCAB-induction was caused by an increase in ATP and chelation of free Mg^{2+}. First, in the presence of a 100-fold excess of Mg^{2+} (10 mM), PstSCAB expression caused a minor reduction in growth rate, but enabled cells to reach the same growth yields as the control strains (Fig. 5*C*). Importantly, Mg^{2+} rescued the growth of the PstSCAB expressing strain even though its ATP levels remained 4-fold higher relative to control strains harboring the empty vector or expressing the plasmid-borne PmrB (Fig. 5*A*). Second, ectopic expression of a plasmid-encoded ATPase (15) rescued the reduction in growth yield caused by PstSCAB-induction (Fig. 5*D*). By contrast, no rescue was observed in cells harboring the vector control (Fig. 5*D*). Taken together, these results indicate that excess Pi imported into the cytoplasm is rapidly assimilated into ATP, causing a decrease in the levels of free cytoplasmic Mg^{2+}, and inhibiting growth.

Excessive Pi uptake impairs translation and promotes MgtC expression during growth in high Mg^{2+}

If excessive Pi uptake leads to physiological conditions resembling cytoplasmic Mg^{2+} starvation (Fig. 5*A-D*) (19, 26, 27), then, increased Pi uptake resulting from the expression of PstSCAB should also decrease translation rates. Furthermore, because a reduction in translation rates caused by cytoplasmic Mg^{2+} starvation promotes *mgtC* transcription (20, 21, 25, 26, 38), excessive Pi uptake should promote MgtC expression.

To test these predictions, we first measured fluorescence over time in otherwise wild-type strains harboring a plasmid-borne *gfp* transcriptional

372 fusion to the promoter and leader regions of *mgtC*, and either an empty vector,
373 the pPmrB, or the pPstSCAB plasmid. We determined that *mgtC-gfp*
374 fluorescence increased one hour following the induction of PstSCAB expression
375 (Fig. 6*A*). This increase in fluorescence was absent or delayed in control strains
376 harboring the empty vector or expressing the plasmid copy of the inner
377 membrane protein PmrB (Fig. 6*A*). [Note that during growth in 25 μM Mg^{2+}, the
378 control strains display a minor increase in fluorescence at 4 h of growth. This
379 small increase in fluorescence results from late onset of cytoplasmic Mg^{2+},
380 which is delayed when compared to cells grown at 10 μM Mg^{2+} (15, 20, 21, 56)].
381 Consistent with the notion that increased ATP production resulting from
382 excessive Pi assimilation disrupts translation by sequestering free Mg^{2+} ions, the
383 effect of PstSCAB expression on the time and fluorescence levels of *mgtC-gfp*
384 was inversely related to the availability of Mg^{2+} in the growth medium.
385 Specifically, fluorescence levels resulting from PstSCAB expression in cultures
386 grown in 25 μM Mg^{2+} were higher than those grown in 50 μM Mg^{2+}, which, in
387 turn, were higher than those grown in 100 μM Mg^{2+} (Fig. 6*A*). Whereas cells
388 grown in 100 μM Mg^{2+} displayed a relatively mild increase in *mgtC-gfp* activity
389 1 h after PstSCAB expression, their fluorescence levels rose rapidly at 7.5 h post
390 induction (Fig. 6*A*). This later induction of *mgtC* expression likely reflects the
391 time point at which cells exhaust the Mg^{2+} available in the growth medium, can
392 no longer neutralize the excess of intracellular Pi incorporated into ATP and,
393 consequently, are unable to efficiently stabilize their ribosomes (26).
394 To directly test if excessive Pi uptake affected ribosome activity, we
395 measured the translation rates of the aforementioned strains following the
396 induction of the plasmid-borne proteins. We determined that during growth in
397 medium containing 25 μM Mg^{2+}, PstSCAB expression caused a 2-fold reduction
398 in translation rates relative to control strains (Fig. 6*B*-*C*). Notably, PstSCAB

399 expression also caused a relative reduction in translation rates during growth in
400 medium containing a 400-fold excess (10 mM) of Mg^{2+} (Fig. 6*B*-*C*). However, at
401 10 mM Mg^{2+}, cellular translation rates were approximately 2-fold higher across
402 all strains (Fig. 6*B*-*C*). Taken together, these results indicate that the rapid
403 assimilation of excessive Pi imported in the cytoplasm reduces levels of free
404 cytoplasmic Mg^{2+}, thereby lowering translation efficiency and promoting MgtC
405 expression.
406
407 **Discussion**
408 **Pi toxicity via disruption of Mg^{2+} homeostasis**
409 During cytoplasmic Mg^{2+} starvation, *Salmonella* expresses the MgtC membrane
410 protein. This protein promotes bacterial growth and viability by virtue of its
411 ability to reduce ATP levels, thereby increasing the concentration of free
412 intracellular Mg^{2+} needed for the functioning of vital Mg^{2+}-dependent processes
413 (19, 21, 25–27). In this work, we demonstrate that MgtC lowers ATP levels by
414 inhibiting Pi uptake (Fig. 2*A*-*C* and 3*B*), thus limiting the availability of an ATP
415 precursor rather than interfering with the enzymatic catalysis of ATP-
416 generating reactions *per se* (Fig. 1*A*-*C* and 2*A*-*C*). We establish that MgtC
417 hinders the activity of a yet unidentified transporter, which functions as the
418 main Pi uptake system in *Salmonella* (Fig. 3*A*-*F*). Finally, we show that, even
419 when cytoplasmic Mg^{2+} is not limiting, excessive Pi uptake leads to increased
420 ATP synthesis, depletion of free cytoplasmic Mg^{2+}, inhibition of translation and
421 growth (Fig. 5*A*-*D* and 6*A*-*C*). These results indicate that bacterial cells control
422 Pi uptake and subsequent assimilation to avoid the depletion of free
423 cytoplasmic Mg^{2+}.
424 The capacity of MgtC to maintain physiological ATP levels during
425 cytoplasmic Mg^{2+} starvation had been so far ascribed to its inhibitory effect on

426 *Salmonella*'s F_1F_o ATP synthase (30). Here, we demonstrate that this inaccurate
427 conclusion resulted from an experimental artifact arising from the propagation
428 of *atpB* strains in a poorly fermentable carbon source (Fig. 1*A-C*). Indeed, the
429 notion that MgtC lowers ATP levels in an F_1F_o ATP synthase-independent
430 fashion has found support on a recent study by an independent group. While
431 also growing cells in a poorly fermentable carbon source, the authors were still
432 able to show that overexpression of MgtC lowers ATP levels in *atpB* mutants
433 (40). Yet, while this study was unable to identify the source of ATP reduction,
434 we now determine its origin. We establish that MgtC limits Pi uptake,
435 simultaneously hindering *all* ATP-generating enzymatic reactions in the cell
436 (Fig. 7).

437 MgtC inhibition of Pi uptake occurs independently of all characterized Pi
438 importers (PitA and PstSCAB) as well as a Pi exporter (YjbB). Interestingly,
439 heterologous MgtC expression in *E. coli* also activates its PhoB/PhoR two-
440 component system (Fig. S2). Three bona fide Pi importers have been described
441 in *E. coli*: PstSCAB, PitA and PitB, which is not present in *Salmonella* (Fig. 3*A*)
442 (1, 51, 57). Notably, *E. coli* strains containing mutations in all these three Pi
443 transport systems are still able to grow on minimal medium with Pi as the only
444 P source (51, 58). This indicates that *E. coli* also encodes a homolog of the Pi
445 transporter that is targeted by MgtC in *Salmonella*. In fact, given that MgtC
446 homologs promote growth in low Mg^{2+} in a large number of distantly related
447 species (32, 59–65) this transporter is likely to be wide spread in bacteria.

448 If MgtC inhibits the activity of a single Pi importer, what then, prevents Pi
449 uptake by other transport systems? Transcription of the high affinity PstSCAB
450 Pi importer is induced by the PhoB/PhoR two-component system in response
451 to a decrease in cytoplasmic Pi. During the initial stages of cytoplasmic Mg^{2+}
452 starvation, the ribosomal subunits are unable to assemble efficiently (26). This

453 leads to a decrease in translation efficiency and a concomitant reduction in ATP
454 hydrolysis and free cytoplasmic Pi, which triggers *pstSCAB* transcription (15).
455 Whereas expression of MgtC leads to inhibition of the main Pi transporter, the
456 expression of MgtA and MgtB results in an influx of Mg^{2+} into the cytoplasm
457 (19-24). This response restores ribosomal subunit assembly and increases
458 translation efficiency (Fig. 7). Efficient ATP consumption by translation
459 reactions (most notably the charging of tRNAs and the synthesis of GTP, which
460 is subsequently used by elongation factors) (26), replenishes intracellular Pi,
461 effectively repressing PhoB/PhoR and *pstSCAB* transcription (15).

462 Transcription of *pitA* is regulated by the availability of Pi:Zn^{2+} salt (66). Yet,
463 in *E. coli*, PitA undergoes post-transcriptional repression during Mg^{2+}
464 starvation. This repression is orchestrated by the Mg^{2+}-sensing PhoP/PhoQ
465 two-component system (67), which, in *Salmonella*, activates transcription of
466 *mgtCB* and *mgtA* (19). Interestingly, growth in low Mg^{2+} decreases *pitA* mRNA
467 levels in both *Salmonella* and *Yersinia pestis* (68, 69). This suggests that inhibition
468 of PitA expression is a common feature of the Mg^{2+} starvation response among
469 enteric bacteria. Because PitA transports M:Pi salts, repression of this gene may
470 also prevent the importation of other metal cations, such as zinc, that can
471 readily replace scarce Mg^{2+} in enzymatic reactions (70–72). In this context, it is
472 interesting to note that the Pho84 Pi transporter of *Saccharomyces cerevisiae* can
473 promote metal toxicity by importing M:Pi salts (73–76).

474 If excessive ATP is toxic during cytoplasmic Mg^{2+} starvation, why then does
475 MgtC function by hindering Pi uptake and not by directly inhibiting ATP-
476 generating enzyme(s)? Depending on the growth condition, the production of
477 ATP via the oxidation of carbon can occur via several distinct pathways, each
478 involving dozens of enzymes (48). While we can conceive that a single protein
479 may have the capacity to directly inhibit a myriad of distinct enzymes,

480 evolution has likely provided cells with a more parsimonious solution for this
481 problem. Because Pi is an ATP precursor, limitation of Pi uptake enables cells
482 to indirectly hinder *all* ATP generating reactions, *independently* from the
483 metabolic pathway(s) used to oxidize the available carbon source(s) (Fig. 1*B* and
484 7). Hence, the inhibition of Pi uptake by MgtC allows *Salmonella* to lower ATP
485 synthesis, eliciting a physiological response to a lethal depletion of cytoplasmic
486 Mg^{2+}, whether carbon is being metabolized via classic glycolysis, the Entner-
487 Doudoroff, the Pentose Phosphate, the Tricarboxylic Acid Cycle or any other
488 energy-generating pathway (Fig. 1*B* and 7).
489
490 **On the activation of PhoR by MgtC**
491 The results presented herein challenge a proposed model of MgtC functionality
492 set forth by Choi *et al*. (77). In this study, the authors hypothesize that MgtC
493 promotes PstSCAB expression and Pi-uptake via the activation of the
494 PhoB/PhoR two-component system through a direct physical interaction
495 between MgtC and the PhoR histidine kinase (77). Several pieces of our data
496 dispute this model and demonstrate that MgtC inhibits Pi uptake to maintain
497 cellular viability during cytoplasmic Mg^{2+} starvation.
498 First, the growth and viability defects of an *mgtC* mutant are due to excess Pi
499 uptake, which is acutely toxic to cells experiencing cytoplasmic Mg^{2+} starvation
500 (Fig. 4*C-D*; see discussion above). Hence, it is hard to envision a model (77)
501 where MgtC would promote the uptake of precisely the compound responsible
502 for growth inhibition and loss of viability in cells lacking *mgtC* (Fig. 4*C-D*). In
503 this light, there are discrepancies that arise in the model proposed by Choi *et al*.
504 due to the lack of both physiological explanations and phenotypic assays to
505 support the conclusion that cells import Pi during cytoplasmic Mg^{2+} starvation
506 (77).

Second, when MgtC is expressed from its normal chromosomal location in response to cytoplasmic Mg^{2+} starvation, PhoB/PhoR activation and *pstSCAB* transcription precede MgtC expression, which persists long after *pstSCAB* transcription is subdued (Fig. S3*A-B*) (15). Hence, during physiologically relevant conditions, MgtC is unlikely to promote *pstSCAB* expression and Pi uptake as proposed (77). Instead, this phenomenon is better explained by the translation defect caused by a transient decrease in free cytoplasmic Mg^{2+}, which is normalized by the activities of MgtA, MgtB and MgtC, expressed after PhoB/PhoR is activated (15, 26). Consistent with this notion, artificial influx of extracellular Pi by ectopic PstSCAB leads to increased ATP synthesis, disruption of free Mg^{2+} pools, inhibition of translation and promotion of *mgtC* transcription (Fig. 5*A-D* and 6*A-C*). This indicates that MgtC is expressed in response to stress(es) generated by increased Pi uptake. Notably, in *E. coli* , cytoplasmic Mg^{2+} starvation also disrupts translation homeostasis (26) and promotes a PhoB/PhoR activation (Fig. S4), even though this organism lacks an MgtC homolog.

Third, when Mg^{2+} is abundant, ectopic MgtC promotes *pstSCAB* expression (Fig. S1) (15). However, in contrast to results presented by Choi *et al*. (77) we established that increased *pstSCAB* transcription observed in this context *does not* lead to significant alterations in intracellular Pi levels (Fig. 3*B*). This is because, under these conditions, *pstSCAB* transcription is a homeostatic response resulting from the inhibition of a main Pi transporter by MgtC (Fig. 2*A-B* and 3*B-F*). These types of regulatory responses are common among multiple transport systems, and can be abolished by eliminating functional redundancy. For instance, while deletion of the house keeping Mg^{2+} transporter *corA* increases the expression of the specialized Mg^{2+} transporter MgtA (78), CorA overexpression repress MgtA production (56). That is, these genetic

534 modifications alter the concentration of cytoplasmic Mg^{2+}, which governs MgtA
535 expression (20, 21). Likewise, deletion of the *pitA* Pi transporter (Fig. S5) or
536 ectopic overexpression of MgtC leads to increased *pstS* transcription (Fig. S1).
537 That is, cells sense and compensate for a shortage in intracellular Pi caused by
538 these genetic alterations and increase expression of the PstSCAB system. In this
539 light, ectopic MgtC expression in wild-type cells leads to a minor reduction in
540 Pi uptake, but severely impairs Pi uptake in strains lacking the Pi transport
541 systems encoded by *pitA*, *pstSCAB* and *yjbB* (Fig. 3*B*).
542 Fourth, substitution of PhoR leucine 421 by an alanine was reported to
543 disrupt PhoR interaction with MgtC, preventing the activation of PhoB/PhoR
544 by cytoplasmic Mg^{2+} starvation (77). We measured PhoB activation in wild-
545 type and $phoR^{L421A}$ strains using a *pstS-gfp* reporter fusion. Interestingly, wild-
546 type and $phoR^{L421A}$ strains displayed similar fluorescence levels, either when
547 MgtC was ectopically induced (Fig. S6*A*), or when it was expressed from its
548 normal chromosomal location during cytoplasmic Mg^{2+} starvation (Fig. S6*B*).
549 Hence, PhoR L421 residue does not participate in a hypothetical MgtC-
550 mediated PhoB/PhoR activation as proposed (77).
551
552 **Pi toxicity and the control of P assimilation**
553 Mutations that increase Pi uptake via the PstSCAB transport system have been
554 shown to inhibit growth in a wide range of bacterial species (1–7). Yet, the
555 underlying molecular basis for this phenomenon has remained elusive. The
556 realization that MgtC promotes growth and viability during cytoplasmic Mg^{2+}
557 starvation (19, 21) by inhibiting Pi uptake (Fig. 2*A-B* and 3*B*) and, consequently,
558 ATP synthesis (Fig. 2*C*) (27) prompted us to examine the physiological basis of
559 Pi toxicity observed in the context of the aforementioned mutations. We
560 established that increased Pi transport via PstSCAB causes a rise in ATP

561 concentrations (Fig. 5*A*). Increased ATP disrupts the pools of free cytoplasmic
562 Mg^{2+} (Fig. 6*A*), thereby inhibiting translation (Fig. 6*B*-*C*), growth (Fig. 5*B*), and
563 precipitating the expression of MgtC when concentrations of Mg^{2+} in the
564 growth medium is sufficiently high to silence its expression (Fig. 6*A*) (20, 21,
565 25). Whereas these results establish that the toxic effects of excessive Pi are
566 manifested following its assimilation into ATP, they shed light into the
567 underlying causes of Pi toxicity and reveal a logic for cellular control of P
568 assimilation. Rapid synthesis of ATP, and ATP-derived highly charged Pi
569 anions such as rRNA and poly-Pi (26, 79, 80), depletes the pools of free
570 cytoplasmic Mg^{2+}. Cells must control Pi uptake because, when biosynthetic
571 precursors are abundant, simultaneous inhibition of all ATP-generating
572 reactions in the cytoplasm cannot be easily attained.
573
574 **Materials and Methods**
575 **Bacterial strains, plasmid constructs, primers, and growth conditions**
576 The bacterial strains and plasmids used in this study are listed in Table S1, and
577 oligonucleotide sequences are presented in Table S2. Single gene knockouts
578 and deletions were carried out as described (81). Mutations generated via this
579 method were subsequently moved into clean genetic backgrounds via phage
580 P22-mediated transduction as described (82). For chromosomal point
581 mutations, detailed strain construction is described below. Bacterial strains
582 used in recombination and transduction experiments were grown in LB
583 medium at 30° C or 37° C (81, 82). When required, the LB medium was
584 supplemented with ampicillin (100 μg/mL), chloramphenicol (20 μg/mL),
585 kanamycin (50 μg/mL), and/or L-arabinose (0.2% wt/vol).
586 Unless stated otherwise, physiological experiments with bacteria were
587 carried out at 37° C with shaking at 250 rpm in MOPS medium (83) lacking

588 $CaCl_2$ (to avoid repression of the PhoP/PhoQ system) (84) and supplemented
589 with 0.1% (w/v) bacto casamino acids (BD Difco), 25 mM glucose, and the
590 indicated amounts of $MgCl_2$ and K_2HPO_4. Experiments were conducted as
591 follows: after overnight (~16- to 20-h) growth in MOPS medium containing 10
592 mM $MgCl_2$ and 2 mM K_2HPO_4, cells washed three times in medium lacking
593 Mg^{2+} and Pi and inoculated (1:100) in fresh medium containing the indicated
594 concentrations of $MgCl_2$ and K_2HPO_4 and propagated for the corresponding
595 amount of time. It should be noted that at a concentration of 0.1% (w/v) bacto
596 casamino acids (BD Difco), the medium already contains ~163 μM Pi. During
597 physiological experiments, selection of plasmids was accomplished by the
598 addition of ampicillin at 100 μg/mL (overnight growth) or 30 μg/mL
599 (experimental condition), chloramphenicol at 20 μg/mL (overnight growth) or
600 10 μg/mL (experimental condition), and/or kanamycin at 50 μg/mL (overnight
601 growth) or 20 μg/mL (experimental condition). Unless specified otherwise,
602 heterologous expression of proteins was achieved by treatment of cultures with
603 250 μM (pMgtC, pPstSCAB) isopropyl β-D-1-thiogalactopyranoside (IPTG).
604 ATPase expression from pBbB2k-AtpAGD was attained without the addition of
605 the inductor.
606
607 **Estimation of intracellular ATP**
608 Intracellular ATP was estimated as described (15). Briefly, luminescence
609 measurements were performed in a SpectraMax i3x plate reader (Molecular
610 Devices) with a BacTiter-Glo Microbial Cell Viability Assay Kit (Promega) in
611 heat-inactivated cells (80° C for 10 min) according to the manufacturers
612 instructions. Protein concentrations in cell samples were estimated using a

Rapid Gold BCA Protein Assay Kit (Pierce). ATP measurements were normalized by the protein content of the samples.

Estimation of intracellular Pi

Total Pi in the samples was estimated from crude cell extracts using the molybdenum blue method as described before (15, 85). The amounts of Pi in the samples were estimated from a standard curve generated from dilutions of a K_2HPO_4 solution of known concentration, and then normalized by the amount of protein present in each reaction.

Phosphate transport assay

Wild-type (14028s) or *mgtC* (EL4) *Salmonella* were grown in MOPS medium containing 10 μM $MgCl_2$ and 500 μM K_2HPO_4 during 3 h. Wild-type (14028s) or Δ3Pi (RB39) cells harboring either pVector or pMgtC were grown in MOPS containing 250 μM $MgCl_2$ and 500 μM K_2HPO_4 until $OD_{600} \approx 0.2$, at which point, MgtC expression was induced for 15 min with the addition of 750 μM IPTG. To assay the transport of Pi, 20 μCi of radioactive Pi solution (10 μL from a 2 mCi $K_2H^{32}PO_4$ at a concentration of 2 mM of $K_2H^{32}PO_4$, PerkinElmer cat. no. NEX055) was added to 1 mL of cell suspension. At the indicated time points, 50 μL of each sample was submitted to rapid filtration through 0.45 μm mixed cellulose ester membrane filters (Whatman) with an applied vacuum. The filters were washed three times with 1 mL of PBS buffer, and subsequently soaked in 5 mL of scintillation fluid (Research Products International). The amount of radioactivity taken up by the cells was determined with a scintillation counter (Triathler multilabel tester, HIDEX) using the ^{32}P-window and by counting each vial for 20 s. Radioactive counts per minute were normalized by protein

content using a Rapid Gold BCA Protein Assay Kit (Pierce). ^{32}Pi uptake of each sample was normalized against the corresponding control in each independent experiment.

Monitoring gene expression via fluorescence

Following overnight growth, bacteria were washed thrice and diluted in 1:100 in 1 mL of MOPS medium containing the appropriate concentrations of Mg^{2+} and Pi, and aliquot as technical replicates or triplicates into black, clear-bottom, 96-well plates (Corning). Two drops of mineral oil were used to seal the wells and prevent evaporation, and cultures were grown at 37° C with auto-mixing in a SpectraMax i3x plate reader (Molecular Devices). At the desired time points, the green fluorescence (excitation 485 nm/emission 535 nm) and absorbance at 600 nm (OD_{600}) from the wells of the plates were read. Fluorescence measurements were normalized by the OD_{600} of the samples.

Construction of plasmid pPstSCAB (pUHE-PstSCAB)

Phusion® High-Fidelity DNA Polymerase (New England Biolabs) was used in a PCR with primers 446 and 447 and *Salmonella* genomic DNA as template. The PCR product was resolved by agarose gel electrophoresis, purified using Monarch® Gel Extraction Kit (New England Biolabs), and ligated into BamHI/HindIII-digested pUHE-21-2-lacIq plasmid (86), using NEBuilder® HiFi DNA Assembly Cloning Kit (New England BioLabs). The assembly reaction was transformed into electrocompetent EC100D *E. coli*. The construct was verified by DNA sequencing using primers 448-452.

Construction of plasmid pATPase (pBbB2K-AtpAGD)

665 Phusion® High-Fidelity DNA Polymerase (New England BioLabs) was used in
666 a PCR with primers 799 and 800 and pUHE-AtpAGD (15) as template. PCR
667 product was resolved by agarose gel electrophoresis, purified using Monarch®
668 Gel Extraction Kit (New England Biolabs), and ligated into BamHI/EcoRI-
669 digested pBbB2k-GFP plasmid (87), using NEBuilder® HiFi DNA Assembly
670 Cloning Kit (New England BioLabs). The assembly reaction was transformed
671 into electrocompetent EC100D *E. coli*. The functionality of the construct was
672 tested by its capacity to decrease ATP levels in a *Salmonella mgtC* mutant strain
673 (EL4) following growth in 10 μM Mg^{2+} medium (15).
674
675 **Construction of plasmid pP*mgtCB*-GFP**
676 Phusion® High-Fidelity DNA Polymerase (New England Biolabs) was used in a
677 PCR with primers W3443 and W3444 and plasmid pGFP303 (25) as template.
678 The PCR product was resolved by agarose gel electrophoresis, purified using
679 Monarch® Gel Extraction Kit (New England Biolabs), and ligated into
680 SalI/HindIII-digested pACYC184 plasmid (88), using NEBuilder® HiFi DNA
681 Assembly Cloning Kit (New England BioLabs). Assembly reactions were
682 transformed into electrocompetent EC100D *E. coli*. The integrity of the construct
683 was verified by DNA sequencing, and its functionality was verified by
684 monitoring fluorescence in wild-type (14028s) *Salmonella* during growth in
685 MOPS medium containing different $MgCl_2$ concentrations (21).
686
687 **Construction of *phoR*^{L421A} strain (MP1665)**
688 Phusion® High-Fidelity DNA Polymerase (New England Biolabs) was used in a
689 PCR with primers 477 and 478 and plasmid pSLC-242 (89) as template. The
690 PCR product was resolved by agarose gel electrophoresis, purified using
691 Monarch® Gel Extraction Kit (New England Biolabs), and integrated into the

chromosome of wild-type (14028s) *Salmonella* via λ-Red-mediated recombination using plasmid pSIM6 as described (81). Recombinant cells containing the insertion were selected on LB supplemented with 20 μg/mL chloramphenicol and 30 mM glucose at 30°C. This insertion was subsequently replaced via a second λ-Red mediated recombination of primer 480 into the chromosome. Cells were recovered for 3 h as described (89) and selected on MOPS medium containing 9.5 mM NH_4Cl as the sole nitrogen source and 30 mM rhamnose as the sole carbon source. The identity of the *phoR*^{L421A} construct was verified by PCR with primers 481 and 482 followed by DNA sequencing. Its functionality was verified by introducing pP*pstS*-GFPc plasmid into this strain, and measuring fluorescence during growth in MOPS containing different K_2HPO_4 concentrations (15).

L-azidohomoalanine (AHA) labeling and quantification

Salmonella strains were grown in MOPS medium supplemented with an amino acids mixture lacking methionine (Mix−Met: 1.6 mM of alanine, glycine, leucine, glutamate and serine, 1.2 mM glutamine and isoleucine, 0.8 mM arginine, asparagine, aspartate, lysine, phenylalanine, proline, threonine and valine, 0.4 mM histidine and tyrosine, and 0.2 mM cysteine and tryptophan), with the indicated $MgCl_2$ and K_2HPO_4 concentrations. At the corresponding timepoints, cultures were labeled with 40 μM of AHA for 30 min (Click Chemistry Tools). At the end of the labeling period, bacterial cultures were treated with 100 μg/mL of chloramphenicol. Cells were collected by centrifugation at 4°C, washed thrice with ice-cold phosphate buffered saline (PBS) and stored at -80°C.

Cell pellets were thawed and re-suspended in a lysis buffer consisting of 50 mM Tris-HCl pH 8.0, 5% glycerol, 0.5% sodium dodecyl sulfate (SDS) and 1x protease inhibitor cocktail (Roche). Cells were lysed in a MiniBeadbeater-96 (BioSpec) and insoluble debris was removed by centrifugation (10 min, 10,000 X *g*, 4°C). Covalent attachment of fluorescent AFDye 488-alkyne (Click Chemistry Tools) to AHA containing proteins was carried out using Click-&-Go™ Protein Reaction Buffer Kit (Click Chemistry Tools) according to the manufacturer's instructions. Protein concentrations were determined using a Pierce BCA Protein Assay Kit (Thermo Fisher Scientific). Fluorescent signals in samples were measured in a SpectraMax i3x plate reader (Molecular Devices) with 480 nm excitation and 520 nm emission wavelengths. The rate of protein synthesis was estimated as the fluorescence signal normalized by the protein content of the sample.

To determine if alterations on protein synthesis were systemic, AF488-labeled samples were separated by SDS-PAGE and fluorescence in gels was captured with an Amersham Imager 680 (GE Healthcare Life Sciences). To ensure that equal amounts of protein were loaded in each lane, gels were subsequently stained using the ProteoSilver™ Plus Silver Stain Kit (Sigma).

MgtC immunoblot analysis

Wild-type (14028s) or *mgtC* (EL4) *Salmonella* were grown in MOPS medium containing 10 μM $MgCl_2$ and 500 μM K_2HPO_4 for the indicated amount of time. Equivalent amounts of bacterial cells normalized by OD_{600} values were collected, washed with PBS, suspended in 0.15 mL SDS sample buffer (Laemmli sample buffer), and boiled. Cell extracts were loaded and resolved using 4–12% NuPAGE gels (Life Technologies). Proteins were then electro-transferred onto nitrocellulose membrane (iBlot; Life Technologies) following the manufacturer's

744 protocol. MgtC was detected using polyclonal anti-MgtC antibody (90) and the
745 secondary antibody, horseradish peroxidase-conjugated anti-mouse IgG
746 fragment (GE). The blots were developed with the SuperSignal West Femto
747 Chemiluminescent system (Pierce) and visualized with an Amersham Imager
748 600 (GE Healthcare Life Sciences). Mouse-anti RpoB antibody (Thermo Fisher
749 Scientific) was used as the loading control.
750
751 **Image acquisition, analysis and manipulation**
752 Plates, gel and membrane images were acquired using an Amersham Imager
753 600 (GE Healthcare Life Sciences). ImageJ software (91) was used to crop the
754 edges and adjust the brightness and contrast of the images. These modifications
755 were simultaneously performed across the entire set images to be shown.
756
757 **Acknowledgments**
758 M. H. P. is supported by grant AI148774 from the National Institutes of Health
759 and funds from The Pennsylvania State University College of Medicine. E.A.G.
760 is supported by grants AI49561 and AI120558 from the National Institutes of
761 Health.
762
763 **References**
764 1. **Wanner BL**. 1996. Phosphorus assimilation and control of the phosphate
765 regulon, p. 1357–81. *In* Neidhardt, FC, Curtiss, R, Ingraham, JL, Lin, ECC,
766 Low, KB, Magasanik, WS, Reznikoff, WS, Riley, M, Scharchter, M,
767 Umbarger, HE (eds.), *Escherichia coli* and *Salmonella*: Cellular and
768 Molecular Biology, 2nd ed. American Society for Microbiology,
769 Washington D.C.

2. **Webb DC**, **Rosenberg H**, **Cox GB**. 1992. Mutational analysis of the *Escherichia coli* phosphate-specific transport system, a member of the traffic ATPase (or ABC) family of membrane transporters. A role for proline residues in transmembrane helices. J Biol Chem **267**:24661–24668.

3. **Steed PM**, **Wanner BL**. 1993. Use of the *rep* technique for allele replacement to construct mutants with deletions of the *pstSCAB-phoU* operon: Evidence of a new role for the PhoU protein in the phosphate regulon. J Bacteriol **175**:6797–6809.

4. **Rice CD**, **Pollard JE**, **Lewis ZT**, **McCleary WR**. 2009. Employment of a promoter-swapping technique shows that PhoU modulates the activity of the $PstSCAB_2$ ABC transporter in *Escherichia coli*. Appl Environ Microbiol **75**:573–582.

5. **Lubin EA**, **Henry JT**, **Fiebig A**, **Crosson S**, **Laub MT**. 2016. Identification of the PhoB regulon and role of PhoU in the phosphate starvation response of *Caulobacter crescentus*. J Bacteriol **198**:187–200.

6. **Zheng JJ**, **Sinha D**, **Wayne KJ**, **Winkler ME**. 2016. Physiological roles of the dual phosphate transporter systems in low and high phosphate conditions and in capsule maintenance of *Streptococcus pneumoniae* D39. Front Cell Infect Microbiol **6**:63.

7. **diCenzo GC**, **Sharthiya H**, **Nanda A**, **Zamani M**, **Finan TM**. 2017. PhoU allows rapid adaptation to high phosphate concentrations by modulating PstSCAB transport rate in *Sinorhizobium meliloti*. J Bacteriol **199**:1–20.

8. **Maguire ME**, **Cowan JA**. 2002. Magnesium chemistry and biochemistry. Biometals **15**:203–10.

9. **Klein DJ**, **Moore PB**, **Steitz TA**. 2004. The contribution of metal ions to the structural stability of the large ribosomal subunit. RNA **10**:1366–79.

10. **Storer AC**, **Cornish-Bowden A**. 1976. Concentration of MgATP2- and other ions in solution. Calculation of the true concentrations of species present in mixtures of associating ions. Biochem J **159**:1–5.

11. **Schneider DA**, **Gaal T**, **Gourse RL**. 2002. NTP-sensing by rRNA promoters in *Escherichia coli* is direct. Proc Natl Acad Sci U S A **99**:8602–7.

12. **Murray HD**, **Schneider DA**, **Gourse RL**. 2003. Control of rRNA expression by small molecules is dynamic and nonredundant. Mol Cell **12**:125–34.

13. **Pontes MH**, **Sevostyanova A**, **Groisman EA**. 2015. When too much ATP is bad for protein synthesis. J Mol Biol **427**:2586–2594.

14. **Gesteland RF**. 1966. Unfolding of *Escherichia coli* ribosomes by removal of magnesium. J Mol Biol **18**:356–71.

15. **Pontes MH**, **Groisman EA**. 2018. Protein synthesis controls phosphate homeostasis. Genes Dev **32**:79–92.

16. **Gillooly JF**, **Allen AP**, **Brown JH**, **Elser JJ**, **Martinez del Rio C**, **Savage VM**, **West GB**, **Woodruff WH**, **Woods HA**. 2005. The metabolic basis of whole-organism RNA and phosphorus content. Proc Natl Acad Sci U S A **102**:11923–7.

17. **Elser JJ**, **Acharya K**, **Kyle M**, **Cotner J**, **Makino W**, **Markow T**, **Watts T**, **Hobbie S**, **Fagan W**, **Schade J**, **Hood J**, **Sterner RW**. 2003. Growth rate-stoichiometry couplings in diverse biota. Ecol Lett **6**:936–943.

817 18. **Bremer H**, **Dennis PP**. 2008. Modulation of chemical composition and
818 other parameters of the cell at different exponential growth rates. EcoSal
819 Plus **3**.

820 19. **Soncini FC**, **García Véscovi E**, **Solomon F**, **Groisman EA**. 1996.
821 Molecular basis of the magnesium deprivation response in *Salmonella*
822 Typhimurium: Identification of PhoP-regulated genes. J Bacteriol
823 **178**:5092–5099.

824 20. **Cromie MJ**, **Shi Y**, **Latifi T**, **Groisman EA**. 2006. An RNA sensor for
825 intracellular Mg^{2+}. Cell **125**:71–84.

826 21. **Spinelli SV**, **Pontel LB**, **García Véscovi E**, **Soncini FC**. 2008. Regulation
827 of magnesium homeostasis in *Salmonella*: Mg^{2+} targets the *mgtA* transcript
828 for degradation by RNase E. FEMS Microbiol Lett **280**:226–234.

829 22. **Groisman EA**, **Hollands K**, **Kriner MA**, **Lee EJ**, **Park SY**, **Pontes MH**.
830 2013. Bacterial Mg^{2+} Homeostasis, Transport, and Virulence. Annu Rev
831 Genet **47**:625–646.

832 23. **Snavely MD**, **Miller CG**, **Maguire ME**. 1991. The *mgtB* Mg^{2+} transport
833 locus of *Salmonella* Typhimurium encodes a P-type ATPase. J Biol Chem
834 **266**:815–23.

835 24. **Tao T**, **Snavely MD**, **Farr SG**, **Maguire ME**. 1995. Magnesium transport
836 in *Salmonella* Typhimurium: *mgtA* encodes a P-type ATPase and is
837 regulated by Mg^{2+} in a manner similar to that of the *mgtB* P-type ATPase.
838 J Bacteriol **177**:2654–62.

839 25. **Lee EJ**, **Groisman EA**. 2012. Control of a *Salmonella* virulence locus by an

ATP-sensing leader messenger RNA. Nature **486**:271–275.

26. **Pontes MH**, **Yeom J**, **Groisman EA**. 2016. Reducing ribosome biosynthesis promotes translation during low Mg^{2+}stress. Mol Cell **64**:480–492.

27. **Pontes MH**, **Lee EJ**, **Choi J**, **Groisman EA**. 2015. *Salmonella* promotes virulence by repressing cellulose production. Proc Natl Acad Sci **112**:5183–5188.

28. **Blanc-Potard AB**, **Groisman EA**. 1997. The *Salmonella selC* locus contains a pathogenicity island mediating intramacrophage survival. EMBO J **16**:5376–5385.

29. **Eriksson S**, **Lucchini S**, **Thompson A**, **Rhen M**, **Hinton J**. 2003. Unravelling the biology of macrophage infection by gene expression profiling of intracellular *Salmonella enterica*. Mol Microbiol **47**:103–118.

30. **Lee EJ**, **Pontes MH**, **Groisman EA**. 2013. A bacterial virulence protein promotes pathogenicity by inhibiting the bacterium' s own F 1 F o ATP synthase. Cell **154**:146–156.

31. **Okuno D**, **Iino R**, **Noji H**. 2011. Rotation and structure of FoF1-ATP synthase. J Biochem **149**:655–64.

32. **Rang C**, **Alix E**, **Felix C**, **Heitz A**, **Tasse L**, **Blanc-Potard AB**. 2007. Dual role of the MgtC virulence factor in host and non-host environments. Mol Microbiol **63**:605–622.

33. **Aung K**, **Lin S**, **Wu C**, **Huang Y**, **Su C**, **Chiou T**. 2006. *pho2*, a phosphate overaccumulator, is caused by a nonsense mutation in a microRNA399

target gene. Plant Physiol **141**:1000–11.

34. **Nguyen TT**, **Quan X**, **Hwang KH**, **Xu S**, **Das R**, **Choi SK**, **Wiederkehr A**, **Wollheim CB**, **Cha SK**, **Park KS**. 2015. Mitochondrial oxidative stress mediates high-phosphate-induced secretory defects and apoptosis in insulin-secreting cells. Am J Physiol - Endocrinol Metab **308**:E933–E941.

35. **Luan M**, **Zhao F**, **Han X**, **Sun G**, **Yang Y**, **Liu J**, **Shi J**, **Fu A**, **Lan W**, **Luan S**. 2019. Vacuolar phosphate transporters contribute to systemic phosphate homeostasis vital for reproductive development in *Arabidopsis*. Plant Physiol **179**:640–655.

36. **Razzaque MS**. 2011. Phosphate toxicity: New insights into an old problem. Clin Sci **120**:91–97.

37. **Lee EJ**, **Groisman EA**. 2012. Tandem attenuators control expression of the *Salmonella mgtCBR* virulence operon. Mol Microbiol **86**:212–224.

38. **Sevostyanova A**, **Groisman EA**. 2015. An RNA motif advances transcription by preventing Rho-dependent termination. Proc Natl Acad Sci U S A **112**:E6835–E6843.

39. **Park M**, **Nam D**, **Kweon D-H**, **Shin D**. 2018. ATP reduction by MgtC and Mg^{2+} homeostasis by MgtA and MgtB enables *Salmonella* to accumulate RpoS upon low cytoplasmic Mg^{2+} stress. Mol Microbiol **110**:283–295.

40. **Park M**, **Kim H**, **Nam D**, **Kweon D**, **Shin D**. 2019. The *mgtCBR* mRNA leader secures growth of *Salmonella* in both host and non-host environments. Front Microbiol **10**:1–12.

41. **Senior AE**. 1990. The proton-translocating ATPase of *Escherichia coli*.

Annu Rev Biophys Biophys Chem **19**.

42. **Harold FM**, **Maloney PC**. 1996. Energy transduction by ion currents, p. 283–306. *In* Neidhardt, FC, Curtiss, R, Ingraham, JL, Lin, ECC, Low, KB, Magasanik, WS, Reznikoff, WS, Riley, M, Scharchter, M, Umbarger, HE (eds.), *Escherichia coli* and *Salmonella*: Cellular and Molecular Biology, 2nd ed. American Society for Microbiology, Washington D.C.

43. **Butlin JD**, **Cox GB**, **Gibson F**. 1973. Oxidative phosphorylation in *Escherichia coli* K-12: the genetic and biochemical characterisations of a strain carrying a mutation in the *uncB* gene. Biochim Biophys Acta **292**:366–375.

44. **Murarka A**, **Dharmadi Y**, **Yazdani SS**, **Gonzalez R**. 2008. Fermentative utilization of glycerol by *Escherichia coli* and its implications for the production of fuels and chemicals. Appl Environ Microbiol **74**:1124–1135.

45. **Richter K**, **Gescher J**. 2014. Accelerated glycerol fermentation in *Escherichia coli* using methanogenic formate consumption. Bioresour Technol **162**:389–91.

46. **Marr AG**. 1991. Growth rate of *Escherichia coli*. Microbiol Rev **55**:316–333.

47. **Russell JB**, **Cook GM**. 1995. Energetics of bacterial growth: Balance of anabolic and catabolic reactions. Microbiol Rev **59**:48–62.

48. **Madigan MT**, **Martinko JM**, **Bender KS**, **Buckley DH**, **Stahl DA**. 2015. Microbial Metabolism, p. 73–96. *In* Brock Biology of Microorganisms, 14th ed. Pearson, Upper Saddle River, NJ.

49. **Rosenberg H**, **Gerdes RG**, **Chegwidden K**. 1977. Two systems for the

uptake of phosphate in *Escherichia coli*. J Bacteriol **131**:505–511.

50. **van Veen HW**, **Abee T**, **Kortstee GJ**, **Konings WN**, **Zehnder AJ**. 1994. Translocation of metal phosphate via the phosphate inorganic transport system of *Escherichia coli*. Biochemistry **33**:1766–70.

51. **Harris RM**, **Webb DC**, **Howitt SM**, **Cox GB**. 2001. Characterization of PitA and PitB from *Escherichia coli*. J Bacteriol **183**:5008–5014.

52. **Cox GB**, **Webb D**, **Rosenberg H**. 1989. Specific amino acid residues in both the PstB and PstC proteins are required for phosphate transport by the *Escherichia coli* Pst system. J Bacteriol **171**:1531–4.

53. **Motomura K**, **Hirota R**, **Ohnaka N**, **Okada M**, **Ikeda T**, **Morohoshi T**, **Ohtake H**, **Kuroda A**. 2011. Overproduction of YjbB reduces the level of polyphosphate in *Escherichia coli*: A hypothetical role of YjbB in phosphate export and polyphosphate accumulation. FEMS Microbiol Lett **320**:25–32.

54. **Gardner SG**, **Johns KD**, **Tanner R**, **McCleary WR**. 2014. The PhoU protein from *Escherichia coli* interacts with PhoR, PstB, and metals to form a phosphate-signaling complex at the membrane. J Bacteriol **196**:1741–1752.

55. **Wanner BL**. 1986. Novel regulatory mutants of the phosphate regulon in *Escherichia coli* K-12. J Mol Biol **191**:39–58.

56. **Cromie MJ**, **Groisman EA**. 2010. Promoter and riboswitch control of the Mg^{2+} transporter MgtA from *Salmonella enterica*. J Bacteriol **192**:604–7.

57. **Hoffer SM**, **Schoondermark P**, **Van Veen HW**, **Tommassen J**. 2001. Activation by gene amplification of *pitB*, encoding a third phosphate

transporter of *Escherichia coli* K-12. J Bacteriol **183**:4659–4663.

58. **Hoffer SM**, **Tommassen J**. 2001. The phosphate-binding protein of *Escherichia coli* is not essential for Pi-regulated expression of the Pho regulon. J Bacteriol **183**:5768–5771.

59. **Buchmeier N**, **Blanc-Potard AB**, **Ehrt S**, **Piddington D**, **Riley L**, **Groisman EA**. 2000. A parallel intraphagosomal survival strategy shared by *Mycobacterium tuberculosis* and *Salmonella enterica*. Mol Microbiol **35**:1375–1382.

60. **Lavigne J**, **O'Callaghan D**, **Blanc-Potard AB**. 2005. Requirement of MgtC for *Brucella suis* intramacrophage growth: a potential mechanism shared by *Salmonella enterica* and *Mycobacterium tuberculosis* for adaptation to a low-Mg^{2+} environment. Infect Immun **73**:3160–3163.

61. **Maloney KE**, **Valvano MA**. 2006. The *mgtC* gene of *Burkholderia cenocepacia* is required for growth under magnesium limitation conditions and intracellular survival in macrophages. Infect Immun **74**:5477–5486.

62. **Belon C**, **Gannoun-Zaki L**, **Lutfalla G**, **Kremer L**, **Blanc-Potard AB**. 2014. *Mycobacterium marinum* MgtC plays a role in phagocytosis but is dispensable for intracellular multiplication. PLoS One **9**:1–23.

63. **Belon C**, **Soscia C**, **Bernut A**, **Laubier A**, **Bleves S**, **Blanc-Potard AB**. 2015. A macrophage subversion factor is shared by intracellular and extracellular pathogens. PLoS Pathog 1–24.

64. **Le Moigne V**, **Belon C**, **Goulard C**, **Accard G**, **Bernut A**, **Pitard B**, **Gaillard JL**, **Kremer L**, **Herrmann JL**, **Blanc-Potard AB**. 2016. MgtC as a

955 host-induced factor and vaccine candidate against *Mycobacterium*
956 *abscessus* infection. Infect Immun **84**:2895–2903.

957 65. **Cafiero JH**, **Lamberti YA**, **Surmann K**, **Vecerek B**, **Rodriguez ME**. 2018.
958 A *Bordetella pertussis* MgtC homolog plays a role in the intracellular
959 survival. PLoS One **13**:1–17.

960 66. **Jackson RJ**, **Binet MRB**, **Lee LJ**, **Ma R**, **Graham AI**, **McLeod CW**, **Poole**
961 **RK**. 2008. Expression of the PitA phosphate/metal transporter of
962 *Escherichia coli* is responsive to zinc and inorganic phosphate levels. FEMS
963 Microbiol Lett **289**:219–24.

964 67. **Yin X**, **Wu Orr M**, **Wang H**, **Hobbs EC**, **Shabalina SA**, **Storz G**. 2019. The
965 small protein MgtS and small RNA MgrR modulate the PitA phosphate
966 symporter to boost intracellular magnesium levels. Mol Microbiol
967 **111**:131–144.

968 68. **Srikumar S**, **Kröger C**, **Hébrard M**, **Colgan A**, **Owen S V**, **Sivasankaran**
969 **SK**, **Cameron ADS**, **Hokamp K**, **Hinton J**. 2015. RNA-seq brings new
970 insights to the intra-macrophage transcriptome of *Salmonella*
971 Typhimurium. PLoS Pathog **11**:e1005262.

972 69. **Perez JC**, **Shin D**, **Zwir I**, **Latifi T**, **Hadley TJ**, **Groisman EA**. 2009.
973 Evolution of a bacterial regulon controlling virulence and Mg^{2+}
974 homeostasis. PLoS Genet **5**:e1000428.

975 70. **Beard SJ**, **Hashim R**, **Wu G**, **Binet MR**, **Hughes MN**, **Poole RK**. 2000.
976 Evidence for the transport of zinc(II) ions via the Pit inorganic phosphate
977 transport system in *Escherichia coli*. FEMS Microbiol Lett **184**:231–5.

978 71. **Dudev T**, **Lim C**. 2003. Principles governing Mg, Ca, and Zn binding and
979 selectivity in proteins. Chem Rev **103**:773–787.

980 72. **Foster AW**, **Osman D**, **Robinson NJ**. 2014. Metal preferences and
981 metallation. J Biol Chem **289**:28095–103.

982 73. **Jensen LT**, **Ajua-Alemanji M**, **Culotta VC**. 2003. The *Saccharomyces*
983 *cerevisiae* high affinity phosphate transporter encoded by PHO84 also
984 functions in manganese homeostasis. J Biol Chem **278**:42036–42040.

985 74. **Rosenfeld L**, **Reddi AR**, **Leung E**, **Aranda K**, **Jensen LT**, **Culotta VC**.
986 2010. The effect of phosphate accumulation on metal ion homeostasis in
987 *Saccharomyces cerevisiae*. J Biol Inorg Chem **15**:1051–1062.

988 75. **Rosenfeld L**, **Culotta VC**. 2012. Phosphate disruption and metal toxicity
989 in *Saccharomyces cerevisiae*: Effects of RAD23 and the histone chaperone
990 HPC2. Biochem Biophys Res Commun **418**:414–419.

991 76. **Ofiteru AM**, **Ruta LL**, **Rotaru C**, **Dumitru I**, **Ene CD**, **Neagoe A**,
992 **Farcasanu IC**. 2012. Overexpression of the PHO84 gene causes heavy
993 metal accumulation and induces Ire1p-dependent unfolded protein
994 response in *Saccharomyces cerevisiae* cells. Appl Microbiol Biotechnol
995 **94**:425–435.

996 77. **Choi S**, **Choi E**, **Cho Y**, **Nam D**, **Lee J**, **Lee EJ**. 2019. The *Salmonella*
997 virulence protein MgtC promotes phosphate uptake inside macrophages.
998 Nat Commun **10**:3326.

999 78. **Papp-Wallace KM**, **Nartea M**, **Kehres DG**, **Porwollik S**, **McClelland M**,
1000 **Libby SJ**, **Fang FC**, **Maguire ME**. 2008. The CorA Mg^{2+} channel is

required for the virulence of *Salmonella enterica* serovar Typhimurium. J Bacteriol **190**:6517–6523.

79. **Rudat AK**, **Pokhrel A**, **Green TJ**, **Gray MJ**. 2018. Mutations in *Escherichia coli* polyphosphate kinase that lead to dramatically increased *in vivo* polyphosphate levels. J Bacteriol **200**.

80. **Li Y**, **Rahman SM**, **Li G**, **Fowle W**, **Nielsen PH**, **Gu AZ**. 2019. The composition and implications of polyphosphate-metal in enhanced biological phosphorus removal systems. Environ Sci Technol **53**:1536–1544.

81. **Datta S**, **Costantino N**, **Court DL**. 2006. A set of recombineering plasmids for gram-negative bacteria. Gene **379**:109–115.

82. **Davis R**, **Bolstein D**, **Roth J**. 1980. Advanced Bacterial Genetics. Cold Spring Harbor Lab Press, Cold Spring Harbor, NY.

83. **Neidhardt FC**, **Bloch PL**, **Smith DF**. 1974. Culture medium for enterobacteria. J Bacteriol **119**:736–747.

84. **García Véscovi E**, **Soncini FC**, **Groisman EA**. 1996. Mg^{2+} as an extracellular signal: environmental regulation of *Salmonella* virulence. Cell **84**:165–174.

85. **Kanno S**, **Cuyas L**, **Javot H**, **Bligny R**, **Gout E**, **Dartevelle T**, **Hanchi M**, **Nakanishi T**, **Thibaud M**, **Nussaume L**. 2016. Performance and limitations of phosphate quantification: guidelines for plant biologists. Plant Cell Physiol **57**.

86. **Soncini FC**, **García Véscovi E**, **Groisman EA**. 1995. Transcriptional

autoregulation of the *Salmonella* Typhimurium *phoPQ* operon. J Bacteriol **177**:4364–4371.

87. **Lee TS**, **Krupa RA**, **Zhang F**, **Hajimorad M**, **Holtz WJ**, **Prasad N**, **Lee SK**, **Keasling JD**. 2011. BglBrick vectors and datasheets: A synthetic biology platform for gene expression. J Biol Eng **5**:12.

88. **Chang AC**, **Cohen SN**. 1978. Construction and characterization of amplifiable multicopy DNA cloning vehicles derived from the P15A cryptic miniplasmid. J Bacteriol **134**:1141–56.

89. **Khetrapal V**, **Mehershahi K**, **Rafee S**, **Chen S**, **Lim CL**, **Chen SL**. 2015. A set of powerful negative selection systems for unmodified Enterobacteriaceae. Nucleic Acids Res **43**:e83.

90. **Moncrief MBC**, **Maguire ME**. 1998. Magnesium and the role of *mgtC* in growth of *Salmonella* Typhimurium. Infect Immun **66**:3802–3809.

91. **Schneider CA**, **Rasband WS**, **Eliceiri KW**. 2012. NIH Image to ImageJ: 25 years of image analysis. Nat Methods **9**:671–5.

92. **Blattner FR**, **Plunkett G**, **Bloch CA**, **Perna NT**, **Burland V**, **Riley M**, **Collado-Vides J**, **Glasner JD**, **Rode CK**, **Mayhew GF**, **Gregor J**, **Davis NW**, **Kirkpatrick HA**, **Goeden MA**, **Rose DJ**, **Mau B**, **Shao Y**. 1997. The complete genome sequence of *Escherichia coli* K-12. Science (80) **277**:1453–1462.

93. **Fields PI**, **Swanson RV**, **Haidaris CG**, **Heffron F**. 1986. Mutants of *Salmonella* Typhimurium that cannot survive within the macrophage are avirulent. Proc Natl Acad Sci U S A **83**:5189–5193.

1047 94. **Cherepanov PP**, **Wackernagel W**. 1995. Gene disruption in *Escherichia*
1048 *coli*: Tc^R and Km^R cassettes with the option of Flp-catalyzed excision of the
1049 antibiotic-resistance determinant. Gene **158**:9–14.

1050 95. **Datsenko KA**, **Wanner BL**. 2000. One-step inactivation of chromosomal
1051 genes in *Escherichia coli* K-12 using PCR products. Proc Natl Acad Sci U S
1052 A **97**:6640–5.

1053 96. **Pontes MH**, **Groisman EA**. 2019. Slow growth determines nonheritable
1054 antibiotic resistance in *Salmonella enterica*. Sci Signal **12**.

1055 97. **Chamnongpol S**, **Groisman EA**. 2002. Mg^{2+} homeostasis and avoidance
1056 of metal toxicity. Mol Microbiol **44**:561–571.

1057 98. **Wösten M**, **Kox L**, **Chamnongpol S**, **Soncini FC**, **Groisman EA**. 2000. A
1058 signal transduction system that responds to extracellular iron. Cell
1059 **103**:113–25.

1060 99. **Andersen JB**, **Sternberg C**, **Poulsen LK**, **Bjorn SP**, **Givskov M**, **Molin S**,
1061 **Bjørn SP**, **Givskov M**, **Molin S**. 1998. New unstable variants of green
1062 fluorescent protein for studies of transient gene expression in bacteria.
1063 Appl Environ Microbiol **64**:2240–2246.

1064

Figures and Tables

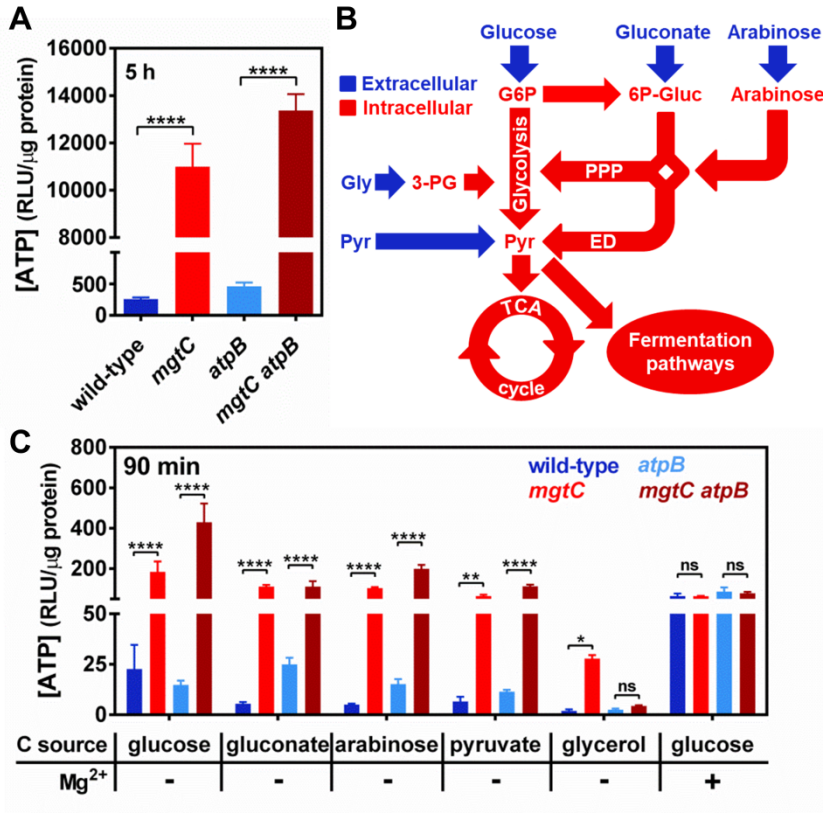

Figure 1. F_1F_O synthase-independent ATP accumulation in an *mgtC* mutant during cytoplasmic Mg^{2+} starvation. *(A)* Intracellular ATP levels in wild-type (14028s), *mgtC* (EL4), *atpB* (MP24) or *mgtC atpB* (MP25) *Salmonella* following 5 h of growth. Cells were grown in MOPS medium containing 10 µM $MgCl_2$ and 2 mM K_2HPO_4. *(B)* Schematic representation of carbon flow through the central metabolic pathways in bacteria with key extracellular (blue) and intracellular (red) metabolites. G6P, glucose-6-phosphate; 6P-Gluc, 6-Phosphogluconate; Gly, glycerol; Pyr, pyruvate; PPP, pentose phosphate pathway; ED, Entner–Doudoroff pathway. *(C)* Intracellular ATP levels in wild-type (14028s), *mgtC* (EL4), *atpB* (MP24) or *mgtC atpB* (MP25) *Salmonella*. Cells were grown in MOPS medium containing 10 mM $MgCl_2$, 2 mM K_2HPO_4 and 25 mM glucose until $OD_{600} \approx 0.4$, washed thrice, and grown for additional 90 min in MOPS medium supplemented with the indicated carbon source (25 mM glucose, 25 mM

sodium gluconate, 30 mM L-arabinose, 50 mM sodium pyruvate, or 50 mM glycerol), and containing 2 mM K_2HPO_4 and either 0 (-) or 10 (+) mM $MgCl_2$. Means ± SDs of three independent experiments are shown. *P < 0.05, **P < 0.01, ****P < 0.0001, and ns, no significant difference. Two-tailed *t* test *(A)*; two-way analysis of variance (ANOVA) with Tukey correction *(C)*.

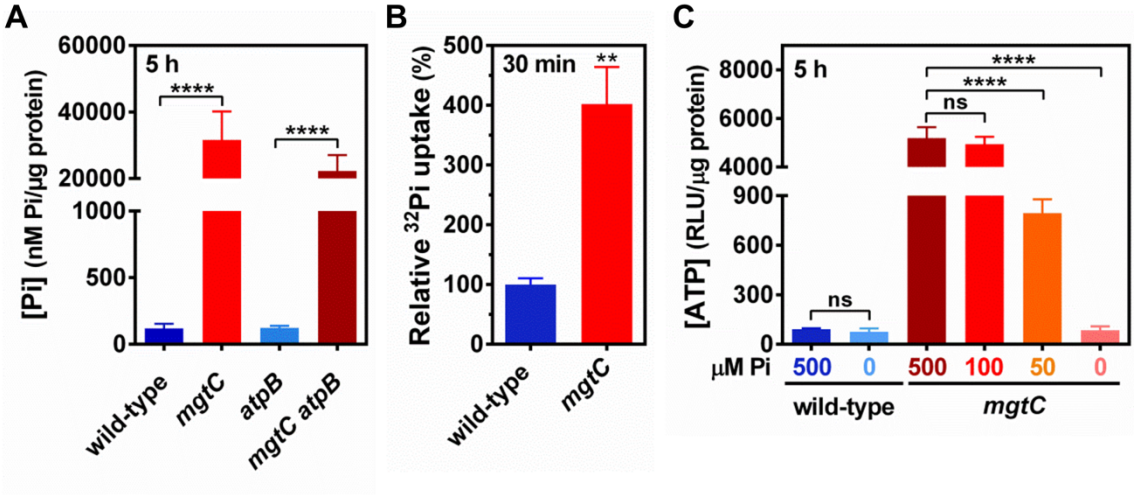

1085

1086 **Figure 2. MgtC-dependent inhibition of Pi transport and assimilation into**
1087 **ATP during cytoplasmic Mg^{2+} starvation.** *(A)* Total intracellular Pi in wild-
1088 type (14028s), *mgtC* (EL4), *atpB* (MP24) or *mgtC atpB* (MP25) *Salmonella*
1089 following 5 h of growth in MOPS medium containing 10 µM $MgCl_2$ and 2 mM
1090 K_2HPO_4. *(B)* Relative radioactive orthophosphate (^{32}Pi) uptake in wild-type
1091 (14028s) or *mgtC* (EL4) cells. Bacteria were grown in MOPS medium containing
1092 10 µM $MgCl_2$ and 500 µM K_2HPO_4 during 3 h before the addition of ^{32}Pi to the
1093 cultures. Levels of ^{32}Pi accumulated in cells were determined after 30 min of
1094 labeling by liquid scintillation counting, as described in Materials and Methods.
1095 ^{32}Pi uptake values were normalized against the wild-type strain. *(C)*
1096 Intracellular ATP levels in wild-type (14028s) or *mgtC* (EL4) *Salmonella*
1097 following 5 h of growth in MOPS medium containing 10 µM $MgCl_2$ and the
1098 indicated concentration of K_2HPO_4 (µM Pi). Means ± SDs of at least three
1099 independent experiments are shown. **$P < 0.01$, ****$P < 0.0001$, and ns, no
1100 significant difference. Two-tailed *t* tests *(A-C)*.

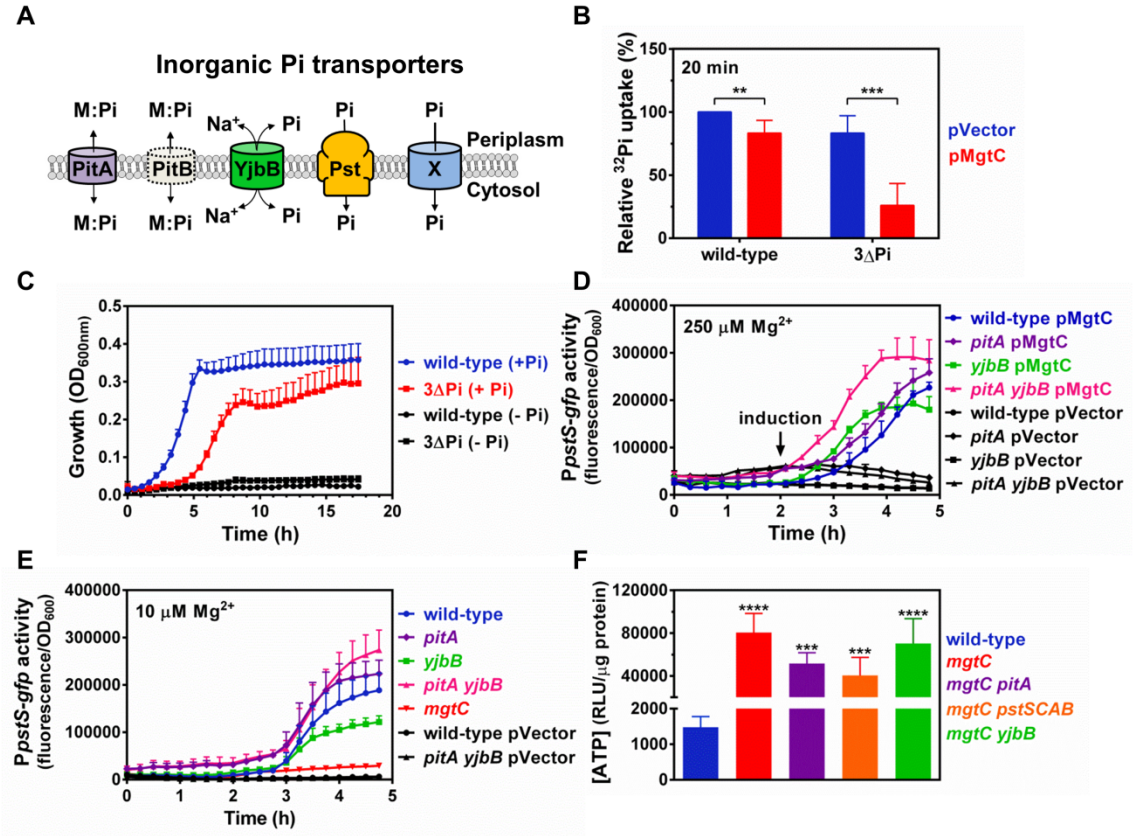

1101

1102 **Figure 3. A non-canonical Pi transport system is inhibited by MgtC.** *(A)*

1103 Schematic representation of inorganic Pi transporters harbored by *Salmonella*

1104 *enterica* and *Escherichia coli*. Note that PitB (grey, dashed outline) is absent from

1105 *Salmonella*. M:Pi, metal-phosphate complex; X, inferred, uncharacterized Pi

1106 transporter inhibited by MgtC. *(B)* Relative ^{32}Pi uptake in wild-type (14028s) or

1107 Δ3Pi (RB39) carrying either pVector (pUHE-21) or pMgtC (pUHE-MgtC).

1108 Bacteria were grown in MOPS medium containing 250 μM $MgCl_2$ and 500 μM

1109 K_2HPO_4 until $OD_{600} \approx 0.2$. Cultures were then propagated for 15 min in the

1110 presence of 750 μM isopropyl β-d-1-thiogalactopyranoside (IPTG) prior to the

1111 addition of ^{32}Pi. Transport of ^{32}Pi was allowed to take place for 20 min.

1112 Intracellular ^{32}Pi accumulation was determined by liquid scintillation counting,

1113 as described in Materials and Methods. ^{32}Pi uptake values were normalized

1114 against the wild-type pVector strain. $^{**}P < 0.01$, $^{***}P < 0.001$, unpaired two

tailed *t* test. *(C)* Growth curve of wild-type (14028s) or Δ3Pi (RB39) *Salmonella*. Cells were grown in MOPS medium uyand containing 10 mM $MgCl_2$ and either 0 (-Pi) or 500 (+Pi) μM of K_2HPO_4. *(D)* Fluorescence from wild-type (14028s), *pitA* (MP1251), *yjbB* (MP1252), *pitA yjbB* (MP1479p) *Salmonella* carrying pP*pstS*-GFPc and either pVector or pMgtC. Cells were grown in MOPS medium containing 250 μM $MgCl_2$ and 500 μM K_2HPO_4. 250 μM of IPTG were added after 2 h of growth. *(E)* Fluorescence from wild-type (14028s), *pitA* (MP1251), *yjbB* (MP1252), *pitA yjbB* (MP1479p), *mgtC* (EL4) *Salmonella* carrying pP*pstS*-GFPc or pVector (the promoterless GFP plasmid pGFPc). Cells were grown in MOPS medium containing 10 μM $MgCl_2$ and 500 μM K_2HPO_4. *(F)* Intracellular ATP levels in wild-type (14028s), *mgtC* (EL4), *mgtC pitA* (MP1254), *mgtC pstSCAB* (MP1720) or *mgtC yjbB* (MP1255) *Salmonella* following 5 h of growth. Cells were grown in MOPS medium containing 10 μM $MgCl_2$ and 2 mM K_2HPO_4. ***$P < 0.001$, ****$P < 0.0001$, unpaired two-tailed *t* tests against the wild-type strain. For all graphs *(B-F)*, means ± SDs of at least three independent experiments are shown.

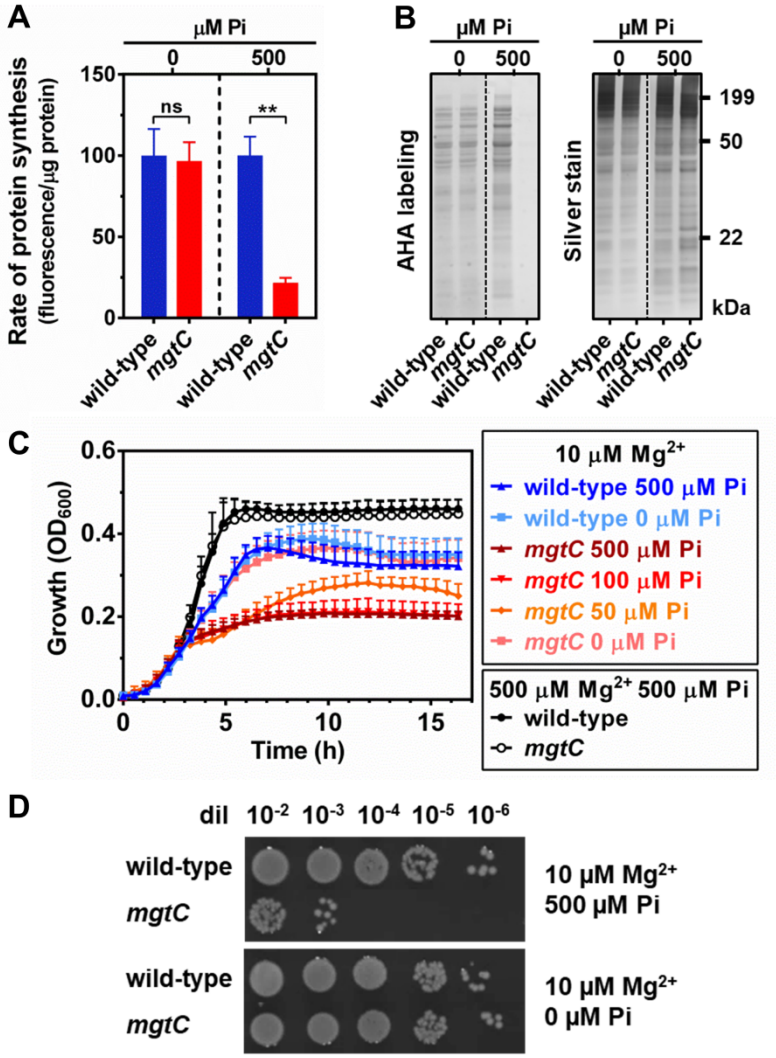

Figure 4. Effect of phosphate limitation on the translation rate, growth and viability of an *mgtC* mutant during cytosolic Mg^{2+} starvation. *(A)* Quantification and *(B)* SDS-PAGE analysis of the rate of protein synthesis [L-azidohomoalanine (AHA) labeling] of wild-type or *mgtC* (EL4) *Salmonella*. Cells were grown in MOPS medium containing 10 mM $MgCl_2$ and 2 mM K_2HPO_4 until $OD_{600} \approx 0.4$. Cells were subsequently washed thrice with MOPS medium lacking $MgCl_2$, K_2HPO_4 and amino acids, and grown for additional 90 min in MOPS medium lacking methionine, and containing 10 μM $MgCl_2$ plus the indicated concentration of K_2HPO_4 (μM Pi). Means ± SDs of four independent experiments are shown. The gel is representative of four independent experiments. Samples from 0 and 500 μM Pi were resolved and imaged from

different gels (indicated by dashed lines). *(C)* Growth curve of wild-type (14028s) or *mgtC* (EL4) *Salmonella*. Cells were grown in MOPS medium containing the indicated concentrations of $MgCl_2$ and K_2HPO_4. Means ± SDs of three independent experiments are shown. *(D)* Viable cell count of wild-type (14028s) or *mgtC* (EL4) *Salmonella* following 16 h of growth in MOPS medium containing 10 μM $MgCl_2$ and 0 or 500 μM K_2HPO_4. Cell suspensions were normalized to the same OD_{600}, diluted, and 5 μL were spotted on plates. Images were taken after incubation of plates at 37°C for 18 h, and are representative of three independent experiments.

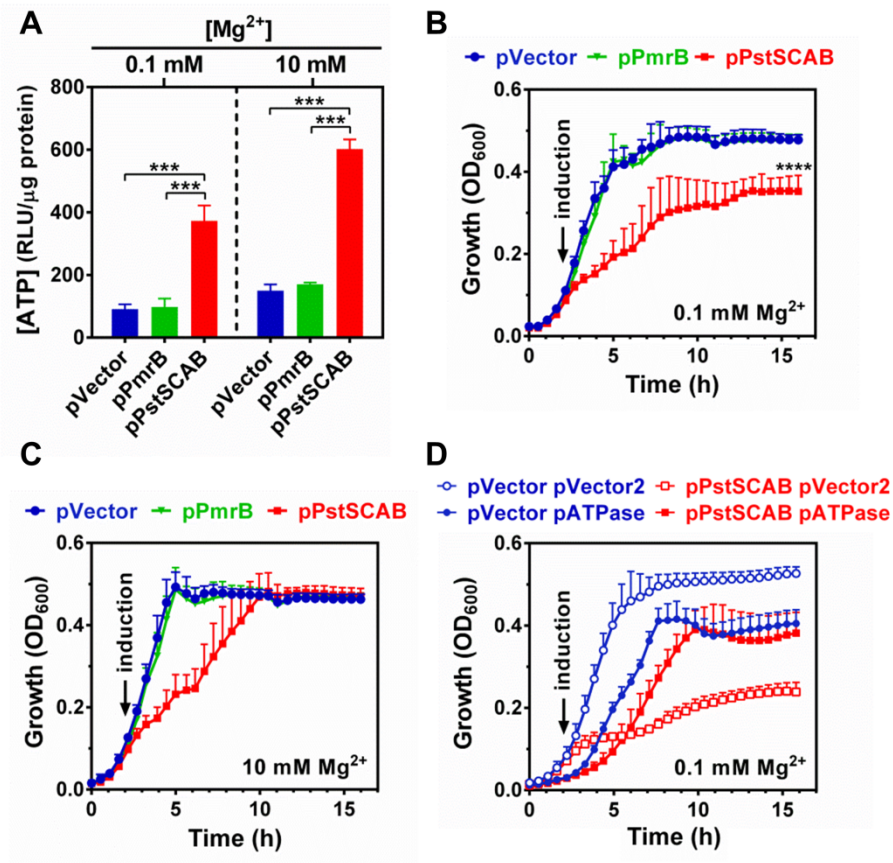

Figure 5. Effect of PstSCAB on growth, P assimilation and Mg^{2+} homeostasis. *(A)* Intracellular ATP levels of cultures depicted in *(B-C)*. Measurements were conducted at 5 h of growth. *(B-C)* Growth curves of wild-type (14028s) *Salmonella* carrying pVector (pUHE-21), pPstSCAB (pUHE-PstSCAB), or pPmrB (pUHE-PmrB) in MOPS medium containing 0.1 (*B*) and 10 mM $MgCl_2$ (*C*). *(D)* Growth curve of wild-type (14028s) *Salmonella* carrying either pVector or pPstSCAB, and either pVector2 (pBbB2K-GFP) or pATPase (pBbB2K-AtpAGD). In all experiments, cells were grown in MOPS medium containing 10 mM K_2HPO_4 and the indicated $MgCl_2$ concentration. Ectopic protein expressions were induced by adding 250 μM IPTG to the cultures after 2 h of growth. Means ± SDs of three independent experiments are shown. *(A-B)* ***P < 0.001, ****P < 0.0001, unpaired two tailed *t* test against pVector.

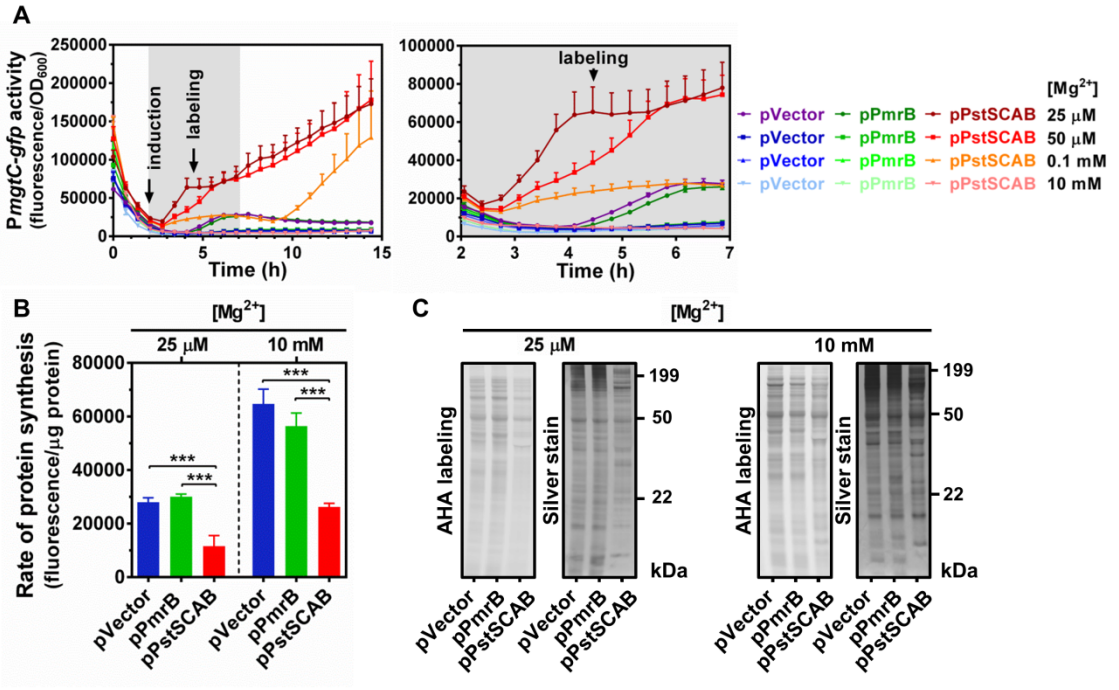

1165

1166 **Figure 6. Effect of PstSCAB expression on *mgtC* transcription and cellular**

1167 **translation rates during grown under conditions of moderate and high Mg^{2+}.**

1168 *(A)* Fluorescence from wild-type (14028s) *Salmonella* carrying transcriptional

1169 reporter pP*mgtC*-GFPc and either pVector (pUHE-21), pPstSCAB (pUHE-

1170 PstSCAB), or pPmrB (pUHE-PmrB). Full time course (left hand-side panel) and

1171 inset between 2 and 7 h (right hand-side panel) of the experiments are shown.

1172 *(B)* Quantification and *(C)* SDS-PAGE analysis of the rate of protein synthesis

1173 [L-azidohomoalanine (AHA) labeling] of wild-type (14028s) *Salmonella* carrying

1174 either pVector, pPmrB or pPstSCAB. In all experiments, cells were grown in

1175 MOPS medium containing 10 mM K_2HPO_4 and the indicated concentration of

1176 $MgCl_2$. For AHA labeling, bacteria were cultured in MOPS medium lacking

1177 methionine (see Materials and Methods). 250 μM IPTG was added to the

1178 cultures following 2 h of growth. AHA was incorporated to the cultures at 4.5

1179 h. Means ± SDs of three independent experiments are shown. Gels are

1180 representative of three independent experiments. ***$P < 0.001$, unpaired two

1181 tailed *t* test against pVector.

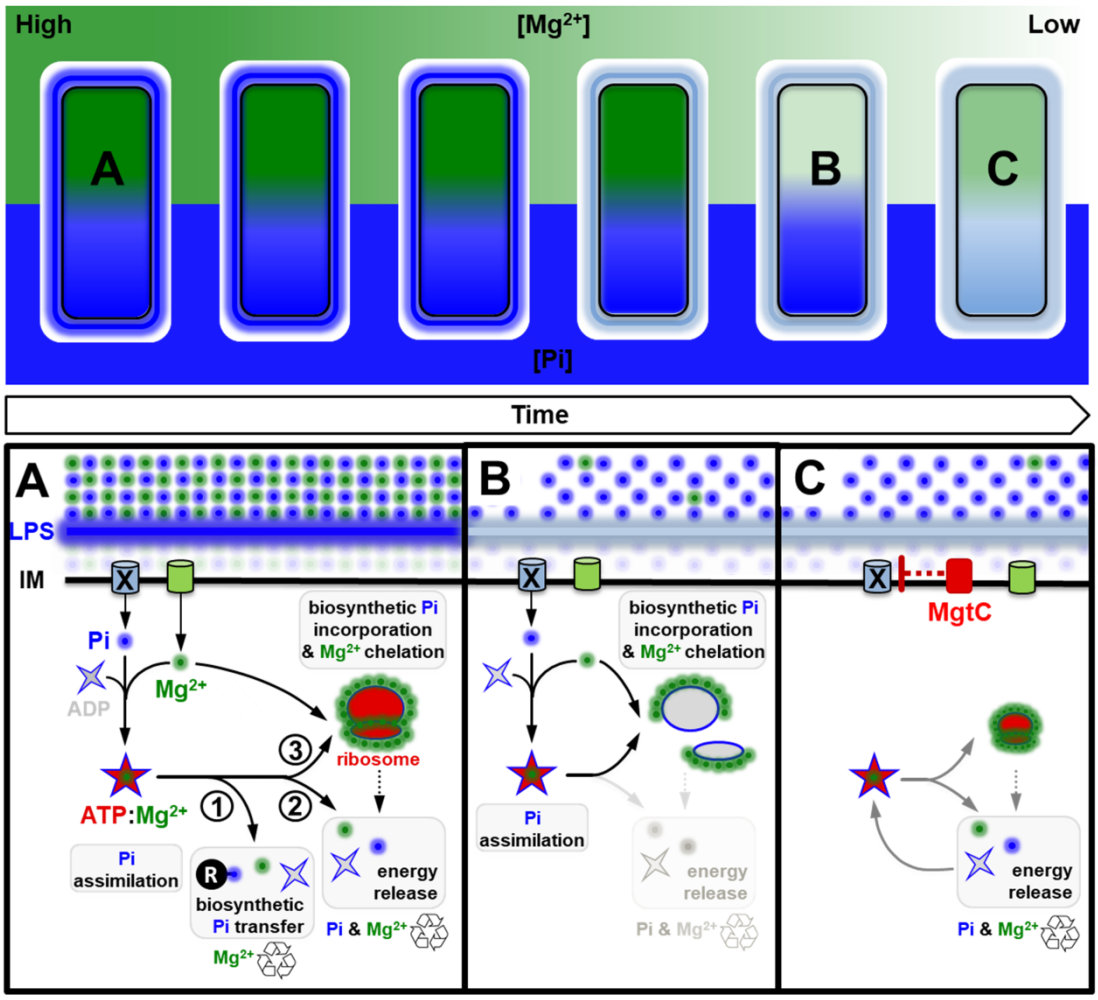

Figure 7. Model illustrating how limitation of phosphate assimilation maintains cytoplasmic Mg^{2+} homeostasis in *Salmonella enterica*. Top panel: Overview of the temporal adaptation of *Salmonella enterica* to Mg^{2+} starvation. Mg^{2+} (green) and Pi (blue) concentrations in the environment, lipopolysaccharide (LPS) and cytoplasm are depicted as gradients with dark colors denoting high concentration and light colors representing low concentrations. Bottom panel: Schematic depicting molecular events and responses underlying the adaptation. *(A)* During homeostasis, Pi is imported into the cytoplasm through dedicated inner membrane (IM) transport systems [X (unknown transporter) and PitA]. Cells assimilate imported Pi through the synthesis of ATP, which exists as a salt with positively charged Mg^{2+}

(ATP:Mg^{2+}). ATP:Mg^{2+} mediates the (1) transfer of Pi among biological molecules, (2) powers energy-dependent enzymatic reactions, and (3) promotes ribosome biogenesis (1). ATP hydrolysis for the release of energy recycles Pi and Mg^{2+}, whereas the biosynthetic transfer of Pi typically recycles cytoplasmic Mg^{2+}. *(B)* After consuming the Mg^{2+} present in the environment, cells eventually experience a shortage in cytoplasmic Mg^{2+} levels (20, 21, 56). Insufficient cytoplasmic Mg^{2+} impairs ribosomal subunit assembly, lowering translation efficiency (26). This reduces the consumption of ATP by translation reactions and, consequently, decreases the recycling of Mg^{2+} and Pi from ATP:Mg^{2+} (15). (*C*) *Salmonella enterica* expresses the MgtC membrane protein as a homeostatic response to cytoplasmic Mg^{2+} starvation. MgtC inhibits Pi uptake through an unknown transporter (X), thereby preventing assimilation Pi into ATP. As the levels of ATP and ribosomes decrease, free Mg^{2+} ions necessary for core processes such as translation are recovered, increasing the efficiency of protein synthesis, and the recycling of Mg^{2+} and Pi from ATP:Mg^{2+}. The density and size of cartoons represent the concentrations of Mg^{2+}, Pi, and ribosomes.

Table S1. Bacterial strains and plasmids used in this study

Strain	Relevant characteristics	Source
Escherichia coli		
EC100D	*pir*$^{+}$ (DHFR) host strain used for generation and propagation of plasmid constructs	Epicentre
MG1655	F^{-} no γδ λS (K12)	(92)
***Salmonella enterica* serovar Typhimurium**		
14028s	wild-type	(93)
EL4	*ΔmgtC*	(30)
MP24	*ΔatpB*::Km^{R}	(93)
MP25	*ΔmgtC ΔatpB*::Km^{R}	This study
MP1251	*ΔpitA*::Ap^{R}	This study
MP1252	*ΔyjbB*::Km^{R}	This study
MP1479p	*ΔpitA*::Ap^{R} *ΔyjbB*::Km^{R}	This study
MP1254	*ΔmgtC ΔpitA*::Ap^{R}	This study
MP1255	*ΔmgtC ΔyjbB*::Km^{R}	This study
MP1720	*ΔmgtC ΔpstSCAB*::Km^{R}	This study
RB39	*ΔpitA ΔpstSCAB*::Km^{R} *ΔyjbB* (3ΔPi)	This study
MP1665	*phoR*^{L421A}	This study
Plasmids		
pSIM6	rep$_{pSC101}$^{ts} Amp^{R} P$_{CI857}$-γβexo	(81)
pCP20	rep$_{pSC101}$^{ts} λ cI857 FLP Amp^{R} Cm^{R}	(94)
pKD4	rep$_{R6K\gamma}$ Amp^{R} FRT Km^{R} FRT	(95)
pKD4-Ap^{r}	rep$_{R6K\gamma}$ Amp^{R} FRT Apr^{R} FRT	(96)
pSLC-242	rep$_{R6K\gamma}$ Amp^{R} FRT Cm^{R} P*rhaB-relE* FRT	(89)
pUHE-21–2-*lacI*^{q}	rep$_{pMB1}$ *lacI*^{q} Amp^{R} vector control	(86)
pUHE-MgtC	rep$_{pMB1}$ *lacI*^{q} Amp^{R} P*lac-mgtC*	(97)
pUHE-PstSCAB	rep$_{pMB1}$ *lacI*^{q} Amp^{R} P*lac-pstSCAB*	This study
pUHE-PmrB	rep$_{pMB1}$ *lacI*^{q} Amp^{R} P*lac-pmrB*	(98)
pGFPc	rep$_{p15A}$ Cm^{R} promoterless *gfp* vector control	(15)
pP*pstS*-GFPc	rep$_{p15A}$ Cm^{R} P*pstS-gfp*	(15)
pP*mgtCB*-GFPc	rep$_{p15A}$ Cm^{R} P*mgtCB-gfp*	This study
pP*phoB*-GFPc	rep$_{p15A}$ Cm^{R} P*phoB-gfp*	(15)
pGFP$_{AAV}$	rep$_{pMB1}$ Amp^{R} promoterless *gfp*$_{AAV}$ vector control	(15)
pP*pstS*-GFP$_{AAV}$	rep$_{pMB1}$ Amp^{R} P*pstS-gfp*$_{AAV}$	(15)
pBbB2k-GFP	rep$_{BBR1}$ Km^{R} *tetR* P*tet-gfp*	(87)
pBbB2K-AtpAGD	rep$_{BBR1}$ Km^{R} *tetR* P*tet-atpAGD*	This study

1214 **Table S2. Oligonucleotides sequences used in this study**

Name	Sequence (5′→ 3′)	Purpose
W3324	AGCGCCTGAAAATGGTATTTATCTGAAATATATAAGAT AAGTGTAGGCTGGAGCTGCTTC	*pitA* inactivation
W3325	TATCCGGCCCATTTGGCTTAAATAATCTTCAGGGAAAGC CATATGAATATCCTCCTTA	*pitA* inactivation
W3326	TCCTCAGTGGTCGCACCAGC	*pitA*::Apr^R verification
W3319	GCTTCAGGAAAACGTATAACGATAAGGAGAACCTGAC GCCGTGTAGGCTGGAGCTGCTTC	*yjbB* inactivation
W3320	GCGCATGTTCTCCGTAGGCCCCGCCATCCGGCATTTCAC CATATGAATATCCTCCTTA	*yjbB* inactivation
W3318	ACGCCAGCAGGCCTTAACGC	*yjbB*::Km^R verification
342	TTTGCTCATCGTAGCAACTCAAACAACGATTTACCGAA ACGTGTAGGCTGGAGCTGCTTC	*pstSCAB* inactivation
343	GGAAATATGTTTATTAAGGTTCAGACTGTCCATTACGCA CTCATATGAATATCCTCCTTA	*pstSCAB* inactivation
340	TGCGCAAACAGTCTAATTC	*pstSCAB*::Km^R verification
143	TGTCCAGATAGCCCAGTAGC	pKD4 inserts verification
446	GAGAAATTAACTATGAGAGGAATGAAAGTTATGCGTAC CA	*pstSCAB* cloning into pUHE-21–2-*lacI*^{q}
447	GTCCAAGCTCAGCTAATTAAGCACGCACTCCTGAATTA ACCG	*pstSCAB* cloning into pUHE-21–2-*lacI*^{q}
448	ATACAGCGCCTTACCGTT	pPstSCAB verification
449	AGGTGACGATGTGTGGCCA	pPstSCAB verification
450	CGTCGATACCACGCGTGAT	pPstSCAB verification
451	TTATCGTCCTGGCGGCGTC	pPstSCAB verification
452	TCGTTCCATAATGCGGCT	pPstSCAB verification
799	CTATCAGTGATAGAGAAAAGAAAATTAACTATGAGAGG AT	*atpAGD* cloning into pBbB2k
800	GAGATCCTTACTCGAGTTTGGATCAGCTAGCTTGGATTC TCAC	*atpAGD* cloning into pBbB2k
W3443	GACAGCTTATCATCGATAAGCTTCTGAATGATCGACCG AGACAG	P*mgtCB-gfp* cloning into pACYC184
W3444	GGCTCTCAAGGGCATCGGTCGACGTTGAGATCCAGTTC GATGTAA	P*mgtCB-gfp* cloning into pACYC184
477	AGTTCGCCTGGCAAAGGAACGCGATTTAGCTTTGTGCAT ATGAATATCCTCCTTA	*phoR*^{L421A} mutation
478	GGCAATTAATCGCTATTTTTGGCAATTAAACGTTCCGGG TGTAGGCTGGAGCTGCTTC	*phoR*^{L421A} mutation
480	AATTAATCGCTATTTTTGGCAATTAAACGTTCCGGCGCC ACAAAGCTAAATCGCGTTCCTTTGCCAGGCGAACT	*phoR*^{L421A} mutation
481	AGTCTTACTGCCTGTGGATG	*phoR*^{L421A} verification
482	ACGCATATTACGGTGAGCT	*phoR*^{L421A} verification

1215

1216

1217

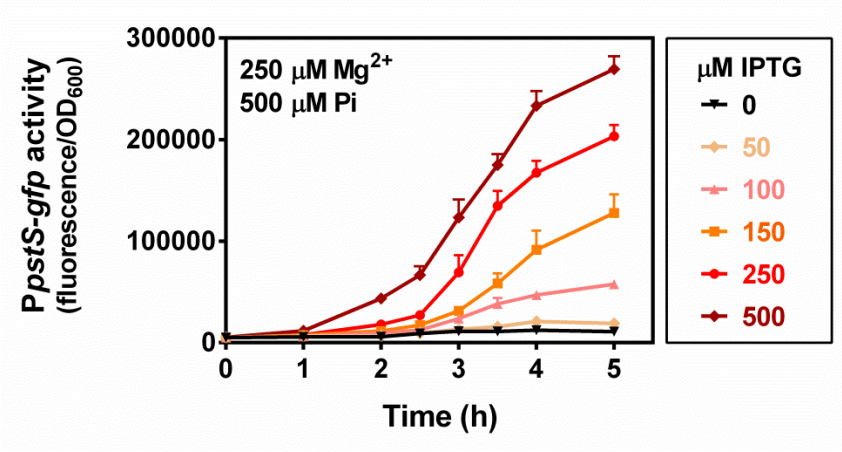

Figure S1. MgtC elicits a dose-dependent activation of the PhoB-activated PstSCAB transporter. Fluorescence from wild-type (14028s) *Salmonella* carrying pP*pstS*-GFPc during growth in MOPS medium containing 250 μM $MgCl_2$, 500 μM K_2HPO_4, and the indicated IPTG concentrations. Means ± SDs of three independent experiments are shown.

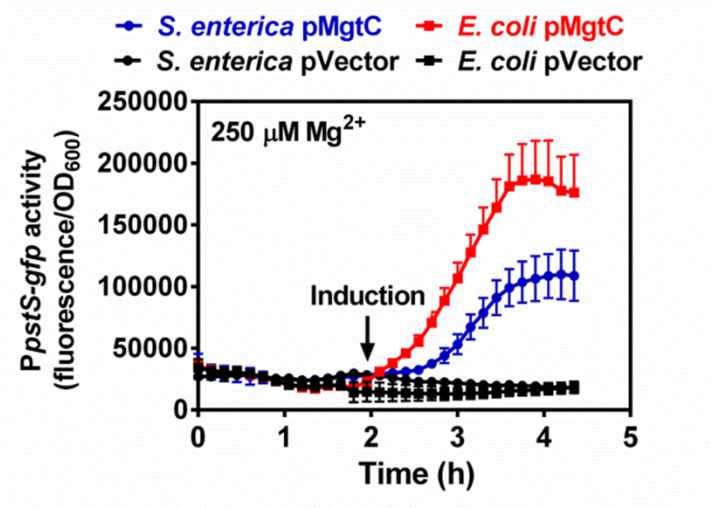

Figure S2. Heterologous expression of *Salmonella* MgtC in *E. coli* activates the PhoB/PhoR two-component system. Fluorescence from wild-type (14028s) *Salmonella enterica*, and wild-type *Escherichia coli* (MG1655) carrying pP*pstS*-GFPc and either pMgtC (pUHE-MgtC) or pVector (pUHE-21). Cells were grown in MOPS medium containing 250 μM $MgCl_2$ and 500 μM K_2HPO_4. 250 μM IPTG was added to the cultures following 2 h of growth. Means ± SDs of three independent experiments are shown.

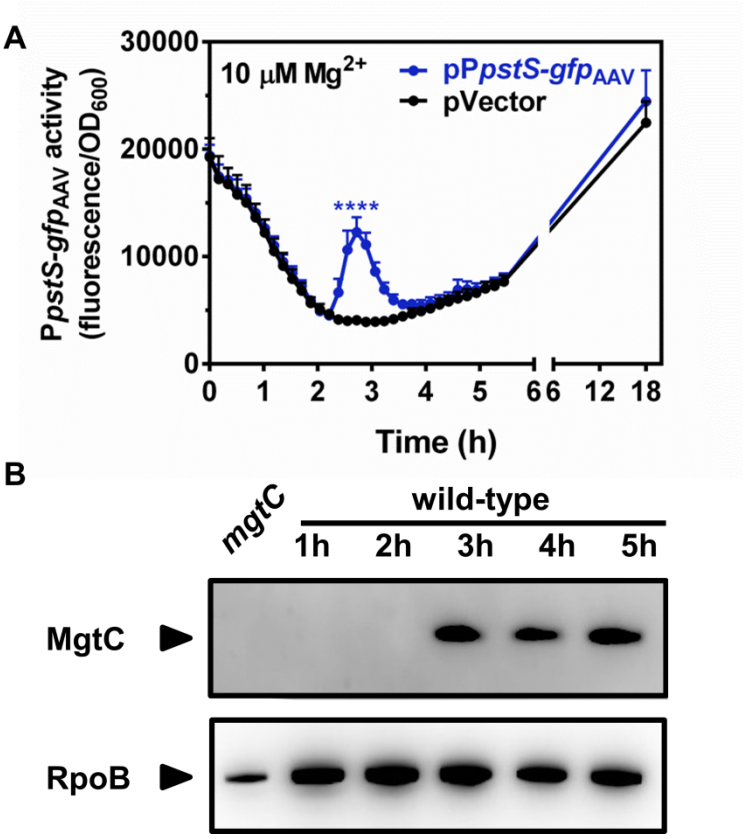

Figure S3. Expression timing of *pstSCAB* and MgtC during cytoplasmic Mg^{2+} starvation. *(A)* Fluorescence from wild-type (14028s) *Salmonella* carrying pP*pstS*-GFP_{AAV} or pVector (the promoterless GFP_{AAV} vector pGFP_{AAV}) plasmid. Note that unstable GFP variants such as GFP_{AAV} enable monitoring of activation and silencing of gene expression (99). Cells were grown in MOPS medium containing 10 μM $MgCl_2$ and 500 μM K_2HPO_4. Means ± SDs are shown. *(B)* Immunoblot analysis using anti-MgtC (upper panel) or anti-RpoB (lower panel, loading control) antibodies of crude extracts prepared from wild-type (14028s) or *mgtC* (EL4) *Salmonella* at the indicated timepoints. Similar expression timings are obtained when transcriptional fusions of *phoB-gfp* and *mgtC-gfp* are used instead (15). For A and B, cells were grown in MOPS medium containing 10 μM $MgCl_2$ and 500 μM K_2HPO_4. Graphs and images are representative of three independent experiments.

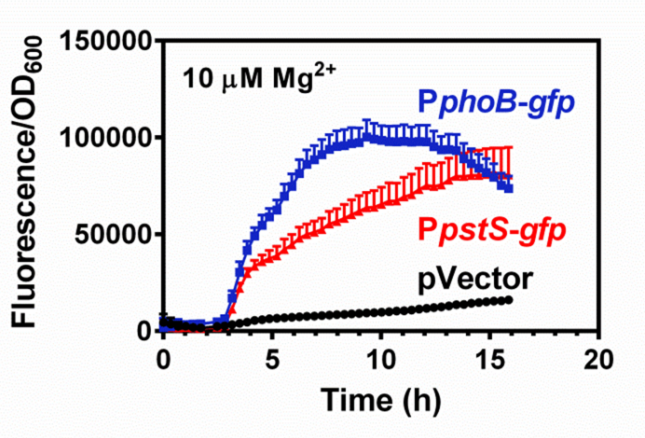

Figure S4. Effect of Mg^{2+} starvation on transcription of *phoB* and *pstSCAB* in *E. coli*. Fluorescence from wild-type (MG1655) *E. coli* carrying pP*phoB*-GFPc, pP*pstS*-GFPc, or pVector (the promoterless GFP plasmid pGFPc). Cells were grown in MOPS medium containing 10 μM $MgCl_2$ and 500 μM K_2HPO_4. Means ± SDs of three independent experiments are shown.

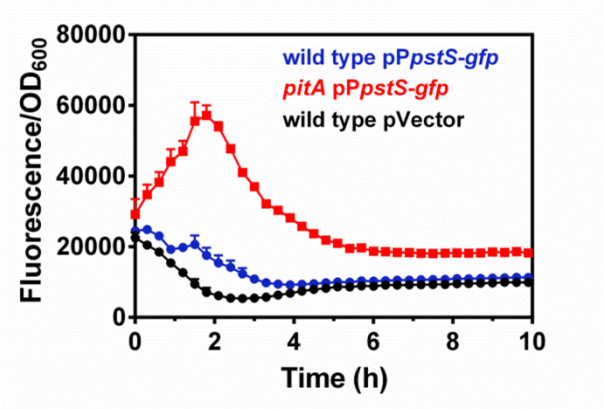

Figure S5. Effect of deleting *pitA* Pi transporter on *pstS* transcription.

Fluorescence from wild-type (14028s) or *pitA* (MP1251) *Salmonella* carrying pP*pstS*-GFPc or pVector (the promoterless GFP plasmid pGFPc). Cells were grown in MOPS medium containing 250 μM $MgCl_2$ and 1000 μM K_2HPO_4. Means ± SDs of three independent experiments are shown.

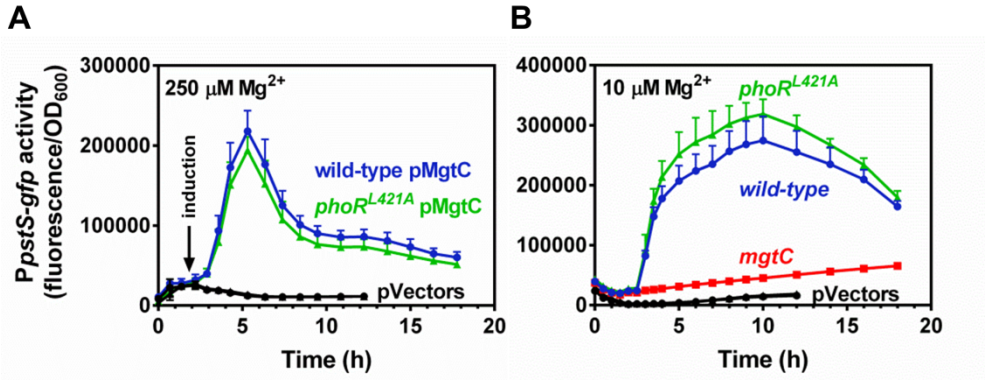

Fig. S6. Effect of *phoR*^{L421A} substitution on the activation of the PhoB/PhoR two-component system. *(A)* Fluorescence from wild-type (14028s) and *phoR*^{L421A} (MP1665) *Salmonella* carrying pP*pstS*-GFPc and either pMgtC (pUHE-MgtC) or pVector (pUHE-21). Cells were grown in MOPS containing 250 μM $MgCl_2$ and 500 μM K_2HPO_4. Following 2 h of growth, 250 μM IPTG was added to the cultures. *(B)* Fluorescence from wild-type (14028s) and *phoR*^{L421A} (MP1665) *Salmonella* carrying pPstS-GFPc or pVector (the promoterless GFP plasmid pGFPc). Cells were grown in MOPS containing 10 μM $MgCl_2$ and 500 μM K_2HPO_4. Means ± SDs of at least three independent experiments are shown.